Huchon, P., Taylor, B., and Klaus, A. (Eds.)
Proceedings of the Ocean Drilling Program, Scientific Results Volume 180

24. Structural Analysis of the Footwall Fault Block of the Moresby Detachment (Woodlark Rift Basin) from Borehole Images[1]

Véronique Louvel,[2] Bernard Le Gall,[3] Bernard Célérier,[4]
Véronique Gardien,[5] and Philippe Huchon[6]

ABSTRACT

During Ocean Drilling Program Leg 180, a north-south transect of sites was drilled in the western Woodlark Basin, a region of active continental extension. This transect is perpendicular to the Moresby detachment system. Moresby Seamount is characterized by the presence of a north-northeast–dipping detachment fault zone on its northern flank. Site 1114 is located near the top of Moresby Seamount in the footwall fault block of the detachment zone. This site is characterized by the presence of an antithetical southwest-dipping normal fault zone putting into contact synrift sediment and highly altered metadolerite.

The Formation MicroScanner (FMS) logging tool provides oriented microresistivity images of the borehole wall. In Hole 1114A, FMS data were recorded from 105 to 297 meters below seafloor (mbsf) through the Pliocene sediment and the sediment/basement contact. The structural analysis of FMS images yields the dips and dip directions of beds and fractures and their density distribution vs. depth.

Three fracture zones (FZs) were determined from FMS images analysis: FZ1 (105–140 mbsf), FZ2 (180–215 mbsf), and FZ3 (270–285 mbsf just above the sediment/basement contact). The fracture zones are characterized by a wide range of fracture dips (10°–80°) and dip directions, but a majority of fractures dip northward and north-northwestward. Within the upper section of FZ2 between 180 and 200 mbsf, fractures clearly dip northward. In this zone, beds are also very well organized

[1]Louvel, V., Le Gall, B., Célérier, B., Gardien, V., and Huchon, P., 2002. Structural analysis of the footwall fault block of the Moresby detachment (Woodlark Rift Basin) from borehole images. *In* Huchon, P., Taylor, B., and Klaus, A. (Eds.), *Proc. ODP, Sci. Results,* 180, 1–43 [Online]. Available from World Wide Web: <http://www-odp.tamu.edu/publications/180_SR/VOLUME/CHAPTERS/165.PDF>. [Cited YYYY-MM-DD
[2]Laboratoire de Mesures en Forage, ODP-NEB, 13545 Aix-en-Provence Cedex 4, France. Present address: 12, Impasse Jean Giono, 13830 Roquefort-La Bedoule, France.
VeroniqueLouvel@aol.com
[3]Institut Universitaire Européen de la Mer, CNRS UMR 6538, 29280 Plouzané, France.
[4]ISTEEM, CNRS-Université de Montpellier II, cc MSE, 34095 Montpellier Cedex 5, France.
[5]Université Lyon I, UMR 5570, 69622 Villeurbanne Cedex, France.
[6]Géosciences Az, Observatorie de Villefranche, BP 48, 06235 Villefranche-sur-mer, France.

Initial receipt: 19 December 2000
Acceptance: 16 May 2002
Web publication: 6 August 2002
Ms 180SR-165

with a northwest dip direction. At 200 mbsf, there is a sharp change of bedding dip direction from northwest above to southwest below. Otherwise, the bedding dip direction is mainly northwest with a west to north distribution. These observations indicate a differential rotation of strata within fault-bounded compartments.

The sediment/basement contact consists of a several-meters-thick tectonic breccia. The contact occurs along a sharp surface dipping at 60° to the southwest.

The presence of strike-slip and oblique faults observed in cores and of reverse faults observed in both cores and FMS images are indicative of an oblique extensional system on Moresby Seamount.

INTRODUCTION

The Woodlark Basin (in Papua New Guinea) is a region where seafloor spreading occurs in its eastern part and active continental rifting in its western part. It is characterized by a westward-propagating rift axis whose current spreading tip is located on the eastern flank of Moresby Seamount, a continental crustal block (Fig. F1). The seafloor magnetic anomalies indicate that seafloor spreading started at 6 Ma at the east of the basin. The western Woodlark Basin provides a good opportunity to study active continental rifting. The seismic profiles indicate the presence of an active low-angle normal detachment fault gently dipping (25°–30°) toward the north-northeast and emerging on the northern flank of Moresby Seamount, the Moresby detachment. Seismic profiles also show the presence of normal faults on the southern flank of Moresby Seamount antithetical to the major low-angle normal fault to the north (Shipboard Scientific Party, 1999a).

The main objective of Ocean Drilling Program (ODP) Leg 180 was to study a region of active continental rifting prior to spreading initiation by drilling the active low-angle Moresby detachment and its subsiding sedimentary hanging wall (Taylor, Huchon, Klaus, et al., 1999). A north-south transect was drilled just ahead of the spreading tip in the rift basin of the northern margin above the low-angle normal fault zone and in the footwall fault block of the Moresby Seamount (Fig. F2). Site 1114, located just north of the crest of Moresby Seamount, is the only site that was logged in the footwall block. Seismic reflection data indicate that sediments are separated from basement by a south-southwest–dipping normal fault at this location.

The objective of this paper is to present the results of the structural analysis of the Formation MicroScanner (FMS) electrical images that were recorded in the footwall of the Moresby detachment in Hole 1114A. A companion paper presents a similar analysis in the northern margin of this detachment, which consists of a large down-flexed sedimentary basin with less deformed prerift/synrift sediments (**Célérier et al.,** this volume). We will first recall the main results of the shipboard core analysis, then show the FMS images and how they relate to the core-defined lithologic units, then discuss the method and results of the structural analysis of these electrical images in the context of the Moresby detachment kinematics.

F1. Leg 180 sites, p. 12.

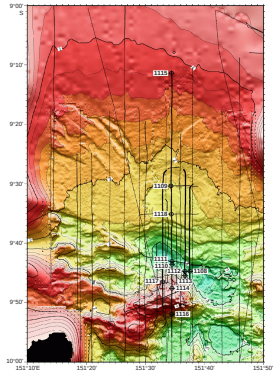

F2. Cross-section of Leg 180 sites, p. 13.

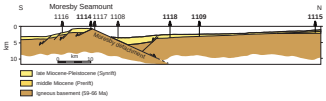

CORE DATA

About 286 m of Pliocene–Pleistocene sediments separated from the metadolerite basement by a 6-m-thick tectonic breccia were drilled in Hole 1114A (Fig. F3). Seven lithologic units were identified within the rift-related, mostly volcaniclastic turbidite sediments (see fig. F1 in Shipboard Scientific Party, 1999c).

Despite the very poor core recovery at Site 1114, structural analysis on cores from the sedimentary section reveals different features of the deformation (Shipboard Scientific Party, 1999c). Deformation is characterized by highly inclined bedding, the presence of faults, and scaly fabrics that increase with depth (Fig. F3).

Bedding measurements show a wide range of dips, from horizontal to 80°, with a majority of dips at 15°. Even if some of the inclined strata may be linked to early soft-sediment deformation, their consistent development throughout the recovered section favors their tectonic origin deformation (Shipboard Scientific Party, 1999c). The increase of the bedding dips with depth is mainly marked from ~110 m deep downward, at the top of the FMS data interval.

Fractures are present all along the cored interval (Fig. F3). Dips range from 0° to 90°, with an average of 30°–40°. Most are dip-slip faults (normal and locally reverse), but oblique and strike-slip faults are also present in the sedimentary section. One of the most characteristic features of the sediments from 64.6 meters below seafloor (mbsf) downward is the presence of scaly fabrics involving fine-grained clay-rich material of various thicknesses. The intensity of fabric development increases with depth. Their origin maybe tectonic or coring induced, but they were interpreted to result mainly from tectonic deformation (Shipboard Scientific Party, 1999c).

However, this core analysis is limited by the poor recovery (~12%) and by the fact that the dip direction of the observed bedding and faults cannot be determined because the cores are not oriented.

FMS DATA

The FMS logging tool applies four pads, each with an array of electrodes, against the formation to produce a continuous oriented map of the electrical microconductivity of the borehole wall (Pezard et al., 1990; Shipboard Scientific Party, 1999b). The FMS calipers indicate the values of two perpendicular diameters of the borehole. The maximum extension of the FMS pads is 15 in, and, if the borehole diameter is larger, the pad contact is poor and the image quality drops.

Two passes of the FMS tool were run in Hole 1114A in an attempt to provide greater coverage of the borehole wall. However, the two images overlie each other over much of the logged interval, as is often the case in noncircular holes. As a consequence, only the second pass, which logged a longer interval, is presented here.

Two types of images were constructed: a dynamic image, where the color equalization is done on a moving 2-m-long window, and a static image, where the color equalization is done for the whole borehole. The FMS images are presented at three different scales, together with the tadpole representation of the structural measurements. First, a synthetic view is provided by whole borehole images at 1/1000 vertical scale (Fig. F4). Only the static image is shown because the 2-m equalization window makes the dynamic images uniform at this scale. The resis-

F3. Core structural features, p. 14.

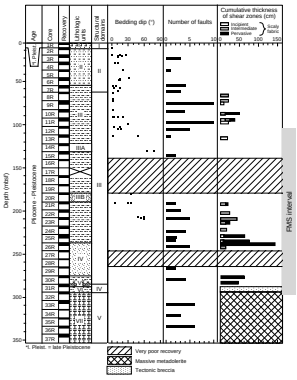

F4. Composite log, p. 15.

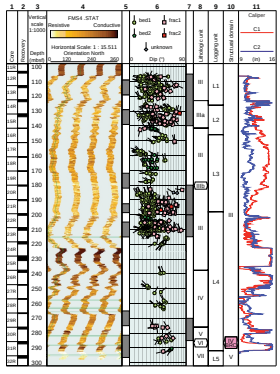

tivity variations in this static image are related to the lithologic variations. Second, full borehole images at the scale of 1/200 are given in the "Appendix," p. 11, for more detailed analysis because this scale is sufficiently small for the borehole image to be limited to a few pages and sufficiently large for the dynamic image to start displaying some character; the color equalization window of 2 m is represented by 1 cm. Finally, close ups of selected intervals at 1/60 to 1/5 scales, which are closer to the typical 1/20 to 1/10 interpretation scales, will illustrate the discussion. The full set of available images and corresponding depth intervals and lithologic units is summarized in Table T1.

The structure of both the sedimentary sequence and the underlying tectonic breccia is almost continuously imaged through a 200-m-long vertical section (105–297 mbsf), with the exception of two large washout zones at 223–234 and 241–247 mbsf (Fig. F4).

The FMS data interval (105–297 mbsf) corresponds, from top to bottom, to lithologic Units III–VII and logging Units L1–L5. Characteristic images facies corresponding to these various units are illustrated. Resistive beds with sharp boundaries are seen within logging Unit L1 (80–126 mbsf) in the upper part of lithologic Unit III (intercalated sandstone, siltstone, and claystone; 55–238 mbsf) (Fig. F5). The increased carbonate content suggested by the higher photoelectric effect of logging Unit L2 (126–146 mbsf) and observed in the calcareous sandstone of Subunit IIIA (123–142 mbsf) corresponds to a zone of higher resistivity in the static image (Fig. F6). A resistive layer with an intricate structure best seen on the static image at 178–180 mbsf (Fig. F7) corresponds to the conglomerate of Subunit IIIB (180–181 mbsf). The lower part (146–238 mbsf) of Unit III shows well-contrasted resistive beds within a more conductive background (Fig. F8).

Within lithologic Unit IV (sandstones; 238–276 mbsf), resistivity is lower than in carbonates and no bedding structure is apparent (Fig. F9). Unit V (silty claystone; 276–286 mbsf), Unit VI (tectonic breccia; 286–287 mbsf), and Unit VII (metadolerite; 287–353 mbsf) FMS facies are shown on Fig. F10, which are degraded by a large washout at 287–292 mbsf.

FMS STRUCTURAL ANALYSIS

The analysis of FMS images complement the observations made of cores. This analysis yields the dip direction of structural events and is not dependent on core recovery. However, it is limited to the depth range outside the two washout zones at 223–234 and 241–247 mbsf.

Planar structures correspond to sinusoids on the images that were mapped with the Schlumberger Geoframe software. They were interpreted either as beds, broken into two categories (bed 1 for best determinations and bed 2 for poorer determinations), fractures (frac 2 for the few faults with reverse offset and frac 1 for the others), or undetermined features (labeled unkn) (Fig. F4). The analysis is usually done on the dynamic image where the corresponding sinusoids are shown (Figs. AF1, F5, F6, F7, F8, F9, F10). The tadpole plot indicates their dip and dip direction. As this hole presents a high density of events, only clearly visible features have been mapped. Several hundreds of unclear features (maybe not planar or present on only one or two pads or impossible to classify in any of the groups, for example) are also present but have not been selected for this study.

T1. Interpreted FMS images, p. 39.

F5. FMS image, 109–119 mbsf, p. 16.

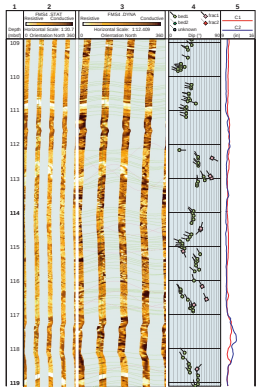

F6. FMS image, 129–139 mbsf, p. 17.

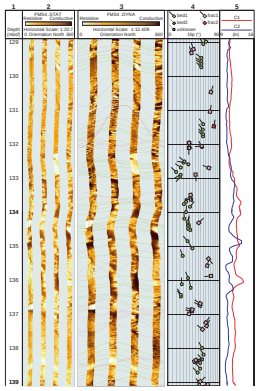

F7. FMS image, 172–182 mbsf, p. 18.

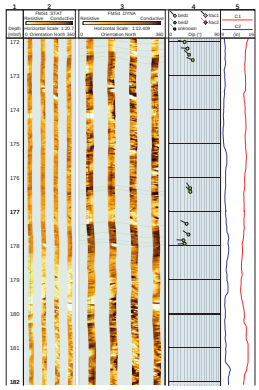

This analysis has led to the determination of 121 fractures (frac 1), three reverse faults (frac 2), 447 beds of good quality (bed 1), 41 beds of poorer quality (bed 2), and three clear but unclassified events (unkn). The depth dependence of the structural measurements is represented on the tadpole plot of the whole borehole images (Fig. F4). The orientation of these measurements is displayed on stereographic projection and on strike and dip histograms (Figs. F11, F12, F13).

DISCUSSION

Fractures

The fractures determined from the Hole 1114A FMS images correspond to either conductive or resistive features, depending on their filling material or on the surrounding formation.

Three major fracture zones (FZs) have been determined from the FMS images analysis: FZ1 (105–140 mbsf), FZ2 (180–215 mbsf), and FZ3 (270–285 mbsf). These fracture zones are clearly expressed on the fractures density (number of fractures per meter) vs. depth plot (Fig. F14). The three fracture zones are composed of structures displaying a wide range of dips, from ~10° to 80°. The orientations shown on stereonets for each fracture zone (Figs. F15, F16, F17) show a wide range of dip directions of random strike. However, the dip direction vs. depth plot of Figure F14 shows a change at 200 mbsf that suggests subdivision of FZ2 into an upper (FZ2a; 180–200 mbsf) (Fig. F18) and lower (FZ2b; 200–215 mbsf) (Fig. F19) section. In the upper section (FZ2a), orientations are concentrated around a 55° dip toward north (Fig. F18).

Between FZ1 and FZ2, no fractures were observed; there are only regular westward to northwestward dipping beds (Figs. F7, AF1), as described below in "Bedding," p. 6. Between FZ2 and FZ3, the two washout zones do not present reliable FMS data. Below the washout zones, no structures, neither bed nor fracture, are observed because of the presence of a massive sandstone (Fig. F9).

Generally, fracture offsets are not visible in Hole 1114A FMS images. However, in three cases small reverse offsets can be observed. The corresponding faults define the set frac 2. Their orientation is shown on the stereonets (Figs. F15, F16). These three reverse faults are located (tadpole plot of Fig. AF1) within FZ1 at 131.5 mbsf and FZ2 at 194.5 and 196.8 mbsf along steep (70° in FZ1 and 42° and 60° in FZ2) northerly dipping fault planes that postdate earlier fault structures. The reverse fault observed in FZ1 at 131.5 mbsf is conductive and crosscuts earlier resistive faults on three FMS pads with a reverse offset of a few millimeters (Fig. F20). At the same depth, an array of reverse microfaults was observed on the recovered sandstones with a similar offset. In FZ2, the observed reverse faults are located at 194.5 and 196.8 mbsf in the upper section FZ2a (180–200 mbsf), where almost all the fractures dip northward (Fig. F18). The reverse faults are conductive and crosscut and shift thicker resistive beds (10–25 cm thick) with an offset of ~20–40 cm (Fig. F21). These zones of reverse faults are locally highly fractured within ~1 m around each reverse fault. Most of the observed events cannot be fitted by sinusoids either because they are not planar or because they are not visible on at least three pads.

Between these two short intervals there is no evidence of offset beds or fractures. It seems that within FZ2a the observed reverse faults are located in short (~1 m long), highly fractured sections and that the inter-

F8. FMS image, 205–215 mbsf, p. 19.

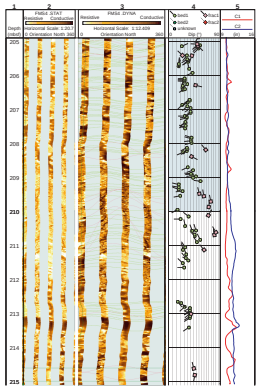

F9. FMS image, 265–275 mbsf, p. 20.

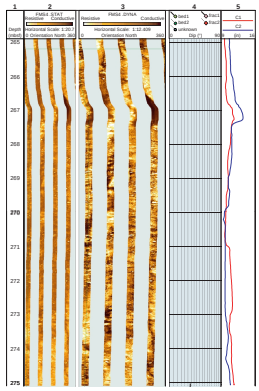

F10. FMS image, 282–296 mbsf, p. 21.

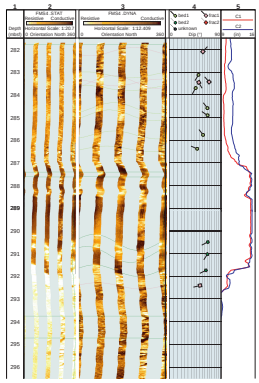

vals between them correspond to ~1.5-m-thick fault-bounded blocks with many fewer fractures. Between 198 and 199.5 mbsf, three northward dipping, very resistive thin beds seem to be also offset with a reverse offset of ~20 cm. However, no associated reverse fault is observed on the FMS images. This succession of short, highly fractured and less fractured intervals can also be observed on the fractures density plot (Fig. F14) with a varying number of fractures with depth within FZ2.

FZ3 corresponds to the zone just above the sediment/tectonic breccia contact and is described below.

Bedding

In the analyzed FMS section, bedding dips between 7° and 65° (Fig. F11). There is no evidence for a general either dip or dip direction vs. depth gradient (Fig. F22). However, the bedding dip direction is mainly northwest over all the logged interval except within FZ2 and suggests the definition of four intervals (B1, B2, B3, and B4) (Fig. F22) to present bed orientation on stereonets (Figs. F23, F24, F25, F26).

In the upper interval (B1; 100–180 mbsf), the bedding dip direction is globally northwest with two principal modes: N285° and N325°, though a wide spectrum of direction is in the northwest quarter (Fig. F23). The dips also present two modes: 15° and 35°. The widest range of dips and dip directions in this zone is located from the top of the FMS record down to ~140 mbsf, which corresponds to the location of FZ1.

The next interval (B2; 180–200 mbsf) is shorter and corresponds exactly to FZ2a. The bed orientations are more concentrated than in the previous interval around a 25° dip toward the northwest at N325° (Fig. F24). Even if this interval is highly fractured, it is very well organized, with a general northward dip direction for the fractures and a general northwestward dip direction for the beds.

Below (B3; 200–225 mbsf), the predominant bedding dip direction changes toward the southwest in the majority, with some beds having a westward dip direction (Fig. F25). The change of dip direction between B2 and B3 at 200 mbsf is very clear and sharp (Fig. F22). The west and southwest dip directions are present throughout the B3 interval except for two very local sets of beds dipping northward at ~205 mbsf and northwestward at 210 mbsf.

The lowest interval (B4; 225–300 mbsf) has ~20 m of washouts with no FMS data (Fig. F22). The beds average dip (45°) is the highest of the four intervals (Fig. F26). The dip direction is northwest in the majority, but a few beds that are parallel to the sediment/basement contact below dip southwestward.

Generally in the depth interval with FMS data, beds are well organized. Their dip direction is mainly northwest, except between 200 and 225 mbsf, where beds mainly dip southwestward. The different bed orientations and their variations seem to be clearly linked to the presence of fracture zones. In FZ1, fractures have an apparent random distribution of dip directions and beds have a wide range of dip and dip directions. In FZ2a, the upper section of FZ2, fractures and beds have a constant orientation. This implies that if the sediments have been rotated or tilted in this zone, this displacement was global. At the bottom of this section (200 mbsf), beds show a sharp change of dip direction that may be due to a stronger tilt of a sedimentary interval linked to this highly fractured 180- to 200-mbsf zone. Below the washout zone, beds recover the general orientation observed above 200 mbsf, with dips increasing with depth.

F11. Global bed orientations, p. 22.

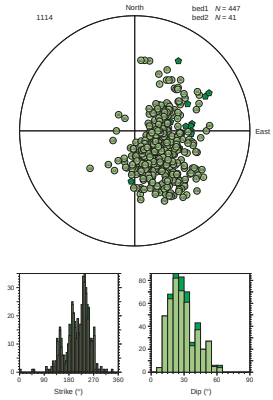

F12. Global fracture orientations, p. 23.

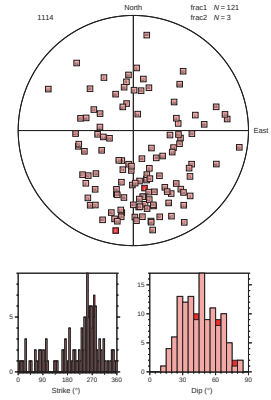

F13. Global unknown planar structure orientations, p. 24.

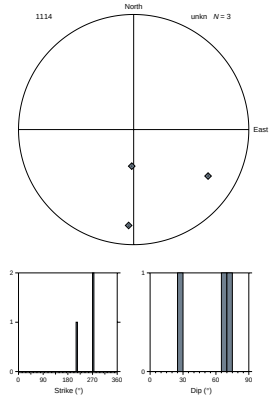

Sediment/Basement Contact

The sediment/basement contact observed on the FMS images at 291 mbsf corresponds to the sediment/tectonic breccia contact which, in turn, corresponds to a south-southwest–dipping fault zone observed on seismic sections and antithetical to the major Moresby detachment. The contact is seen very clearly on the statically normalized FMS image, with a strong resistivity contrast (Fig. F4). Indeed, the recovered breccia consists of highly brecciated metadoleritic basement rocks that form a steeply dipping extensional fault zone. These rocks are much more resistive than the overlying sediment. The dynamically normalized image shows that the tectonic breccia seems to have a centimeter-scale texture similar to the overlying sandstone. The sediment/breccia contact is present within or at the bottom of a washout zone (287–291 mbsf). The orientation of the washout zone boundaries very likely reflects the contact dip direction. The sediment/breccia contact is present along a surface dipping at 60° to the southwest, antithetical to the Moresby detachment. A few planar events (23) have been selected in the tectonic breccia on the FMS images. They have a wide range of dip and dip directions, but the majority of structures dip southwestward, which is consistent with the sediment/breccia contact orientation. This confirms the south-southwest dip direction of the whole fault zone.

The brecciated fault zone thickness is between 5 and 16.5 m from the combination of core and FMS results. The uncertainty is due to the low core recovery and to the washout zones and nearness to the bottom of the record for FMS data. The top of the fault zone may be located between 286 and 294.1 mbsf from cores and between 287 and 291.5 mbsf from FMS data. The bottom may be located between 287.35 and 303.54 mbsf from cores and at least at 296.5 mbsf from FMS data (bottom of the record).

CONCLUSIONS

Any comparison between core and FMS structural analysis results is made difficult by the very poor core recovery in Hole 1114A, the short FMS record interval, and the washout zones in the FMS data. Three fracture zones are clearly determined from FMS images analysis, whereas the distribution of fractures observed on cores shows a nearly constant density of fractures. Between FZ1 and FZ2 determined from FMS images, there is almost no core recovery, so no comparison is possible. Unfortunately, in the interval with significant shear zones evident in cores, there are no reliable FMS data because of washout zones. As for the bedding, dip is much greater below ~100 mbsf in cores, whereas there are no FMS data above. However, the FMS data analysis confirms the presence of bedding dips between ~10° and 60° as observed in cores.

Both cores and FMS data reveal the presence of highly deformed intervals with the presence of shear zones and fracture zones. Reverse faults have also been observed in both sets of data. Thus, although cores and FMS images are not directly comparable, the results of the structural analysis performed on both data are somewhat consistent. An interpretative structural log can be derived from cores and FMS analyses (Fig. F27). It summarizes the evolution of bedding dips with depth from cores and FMS measurements as well as the location of fracture zones determined from FMS images. The wide range of bedding dips observed in the logged sedimentary sequence as well as the sharp changes of bed-

F14. Fracture dip, dip direction, and density vs. depth, p. 25.

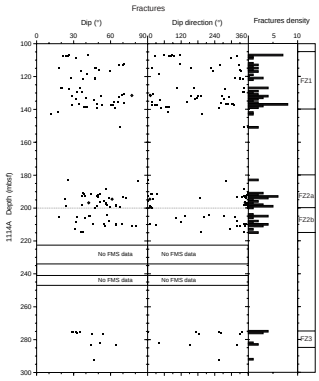

F15. FZ1 fracture orientations, p. 26.

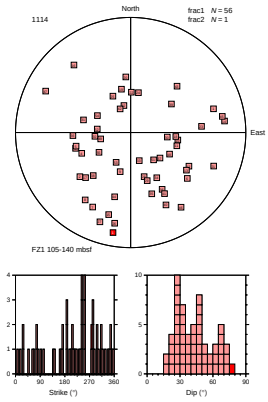

F16. FZ2 fracture orientations, p. 27.

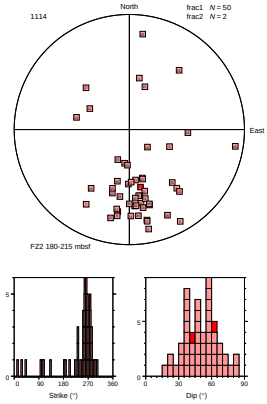

ding dip direction, associated with intense networks of steep faults, may indicate differential rotation of strata within fault-bounded compartments.

The oriented FMS images permit the determination of bed and fracture dip directions. This permits placement of the studied site in a more regional context. Fractures mainly dip north-northwestward and clearly northward in FZ2a. This may express the present north-south extension of the western Woodlark Basin. The presence of strike-slip and oblique faults observed in cores and reverse faults observed on FMS images are indicative of an oblique extensional system on Moresby Seamount that is characterized by the presence of a northeast-dipping detachment zone on its northern flank and by the presence of southwest-dipping antithetical normal faults on its southern flank.

ACKNOWLEDGMENTS

This research used samples and/or data provided by the Ocean Drilling Program (ODP). ODP is sponsored by the U.S. National Science Foundation (NSF) and participating countries under management of Joint Oceanographic Institutions (JOI), Inc. Funding for this research was provided by the CNRS-INSU Géosciences Marines program.

F17. FZ3 fracture orientations, p. 28.

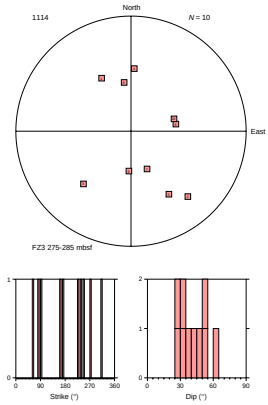

F18. FZ2a fracture orientations, p. 29.

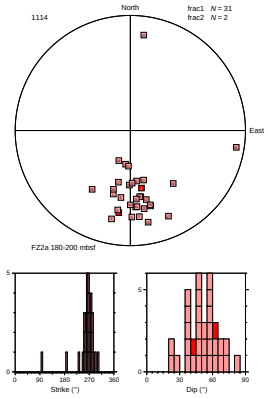

F19. FZ2b fracture orientations, p. 30.

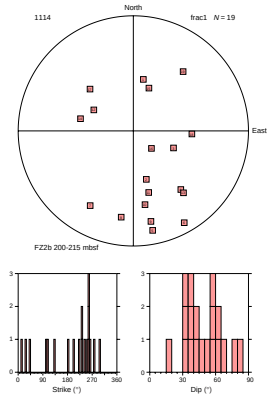

F20. Reverse fault in FZ1, p. 31.

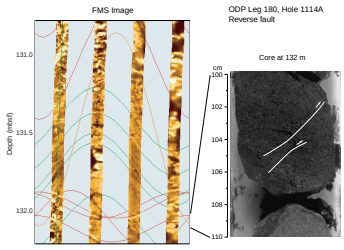

F21. Two reverse faults in FZ2, p. 32.

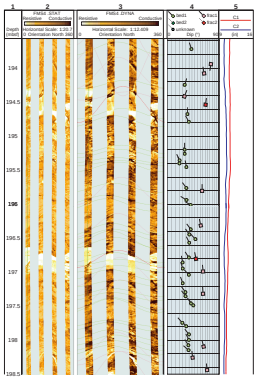

F22. Bedding dip and dip direction vs. depth, p. 33.

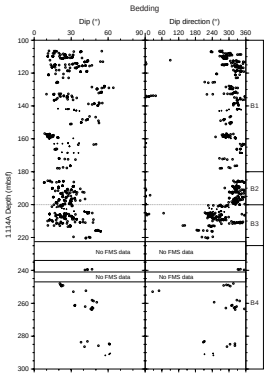

F23. B1 bedding orientations, p. 34.

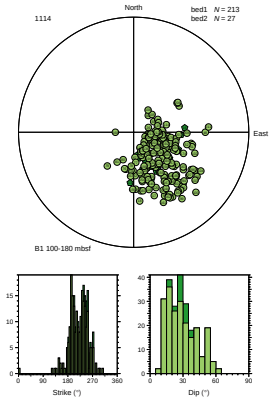

F24. B2 bedding orientations, p. 35.

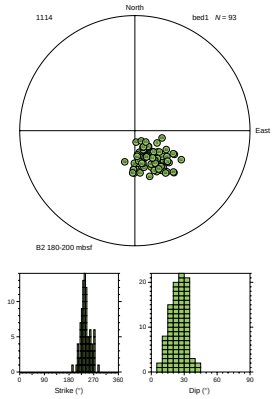

F25. B3 bedding orientations, p. 36.

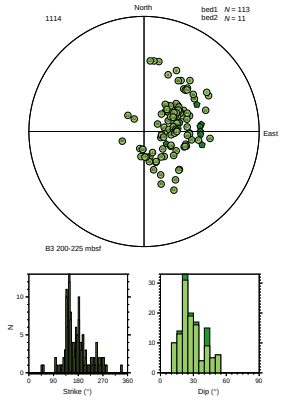

F26. B4 bedding orientations, p. 37.

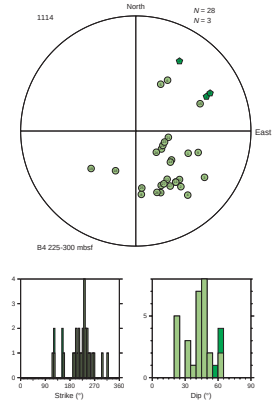

F27. Interpretative structural log, p. 38.

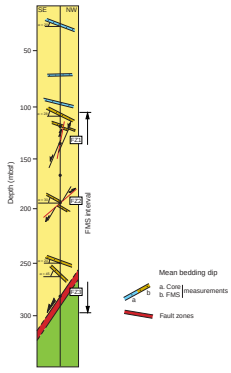

REFERENCES

Goodliffe, A.M., Taylor, B., and Martinez, F., 1999. Data report: Marine geophysical surveys of the Woodlark Basin region. *In* Taylor, B., Huchon, P., Klaus, A. et al., *Proc. ODP Init. Repts.,* 180, 1–20 [CD-ROM]. Available from: Ocean Drilling Program, Texas A&M University, College Station, TX 77845-9547, U.S.A.

Pezard, P.A., Lovell, M., Fujioka, K., Taylor, B., Janecek, T., Aitchison, J.C., Cisowski, S., Colella, A., Cooper, P.A., Klaus, A., Dadey, K.A., Egeberg, P., Firth, J., Isiminger, K.M., Gill, J.B., Herman, Y., Hiscott, R.N., Kaiho, K., Koyama, M., Lapierre, H., Marsaglia, K., Nishimura, A., Rodolfo, K.S., Taylor, R., Tazaki, K., and Torssander, P., 1990. Downhole images: electrical scanning reveals the nature of subsurface oceanic crust. *Eos, Trans. Am. Geophys. Union,* 71:709.

Shipboard Scientific Party, 1999a. Leg 180 summary. *In* Taylor, B., Huchon, P., Klaus, A., et al., *Proc. ODP, Init. Repts.,* 180, 1–77 [CD-ROM]. Available from: Ocean Drilling Program, Texas A&M University, College Station, TX 77845-9547, U.S.A.

————, 1999b. Explanatory notes. *In* Taylor, B., Huchon, P., Klaus, A., et al., *Proc. ODP, Init. Repts.,* 180, 1–75 [CD-ROM]. Available from: Ocean Drilling Program, Texas A&M University, College Station, TX 77845-9547, U.S.A.

————, 1999c. Site 1114. *In* Taylor, B., Huchon, P., Klaus, A., et al., *Proc. ODP, Init. Repts.,* 180, 1–139 [CD-ROM]. Available from: Ocean Drilling Program, Texas A&M University, College Station, TX 77845-9547, U.S.A.

Taylor, B., Huchon, P., Klaus, A., et al., 1999. *Proc. ODP, Init. Repts.,* 180 [CD-ROM]. Available from: Ocean Drilling Program, Texas A&M University, College Station, TX 77845-9547, U.S.A.

APPENDIX

Depth Correlation

The FMS data are processed separately from the conventional logs. In particular, the depth computation includes a sticking detection procedure that uses the tool accelerometer data to correct the winch cable depth data when the tool gets stuck and the measurements conflict. This correction is applied from the bottom of the hole, which is set to be consistent with that of the other logs, and can accumulate significant depth differences upward in some instances. As a consequence, the caliper data that have been processed with the FMS are systematically displayed here so as to correlate observations on the FMS images with those classical logs that also display caliper data. This offset remains small in this hole and can be estimated by comparing the caliper recording shown on Fig. AF1 with that of the triple combination tool string shown in fig. F53A of Shipboard Scientific Party (1999c). The distinctive caliper variations at 107.6, 201.9, and 234.9 mbsf on Figure AF1 are found within 10, 90, and 30 cm on figure 53A of Shipboard Scientific Party (1999c).

FMS Images

This appendix provides a full-image coverage of the borehole at 1/200 scale (Fig. AF1). This scale is sufficiently large for the dynamic image to start displaying variations related to lithology (the sliding color equalization window of 2 m is represented by 1 cm) and sufficiently small for the borehole to be represented in a few pages. Structural measurements and lithology with depth are also shown.

AF1. FMS image and analysis, p. 40.

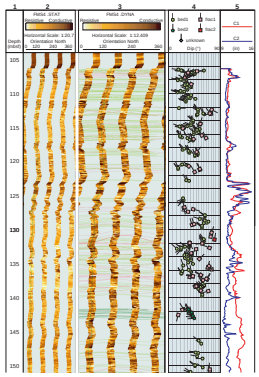

Figure F1. ODP Leg 180 drilled site location map in the Woodlark Basin (from Goodliffe et al., 1999).

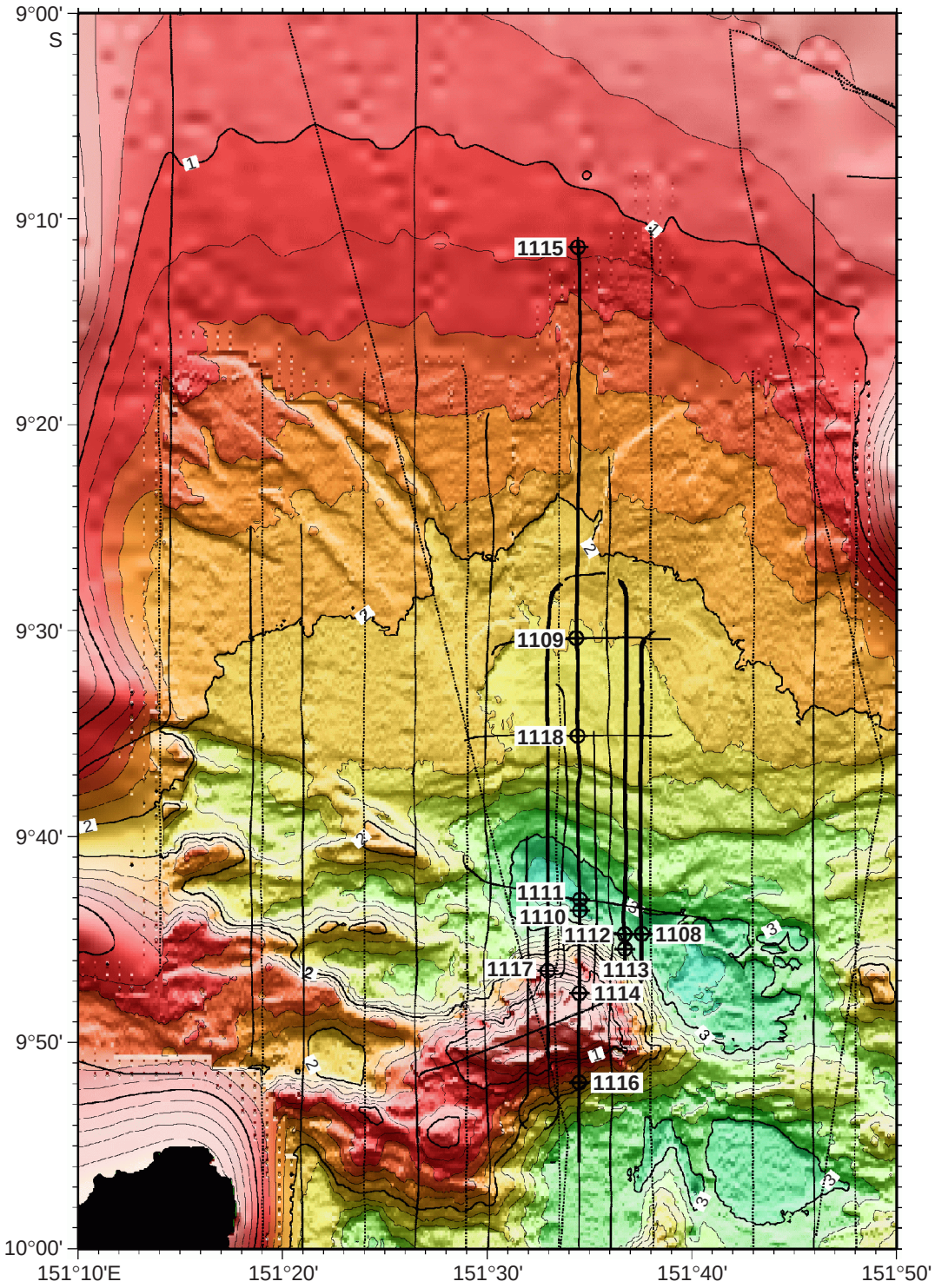

Figure F2. Schematic cross section of Leg 180 sites. Sites logged with the FMS are highlighted in bold. Only Site 1115 reached prerift sediments (modified from Shipboard Scientific Party, 1999b; **Taylor and Huchon,** this volume).

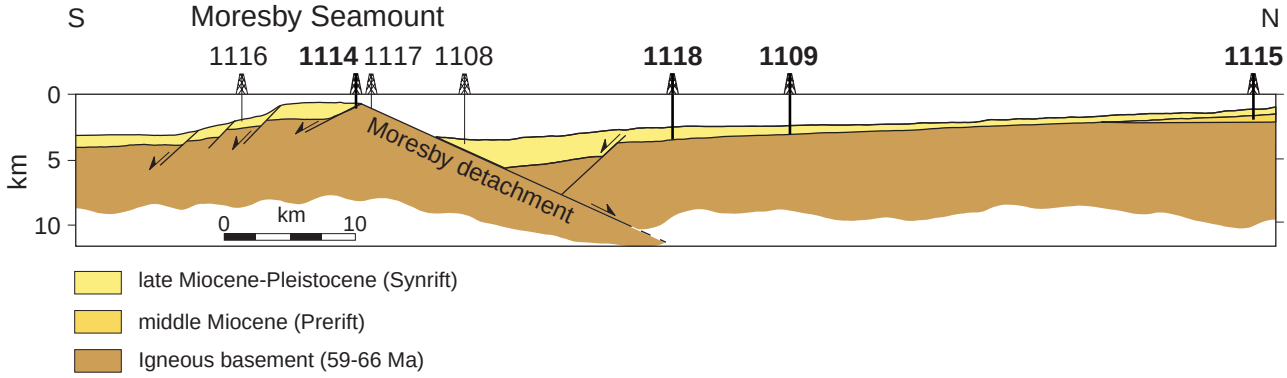

Figure F3. Summary of the main structural features observed in cores at Site 1114. The depth interval logged with the FMS is shown on the right (modified after Shipboard Scientific Party, 1999c).

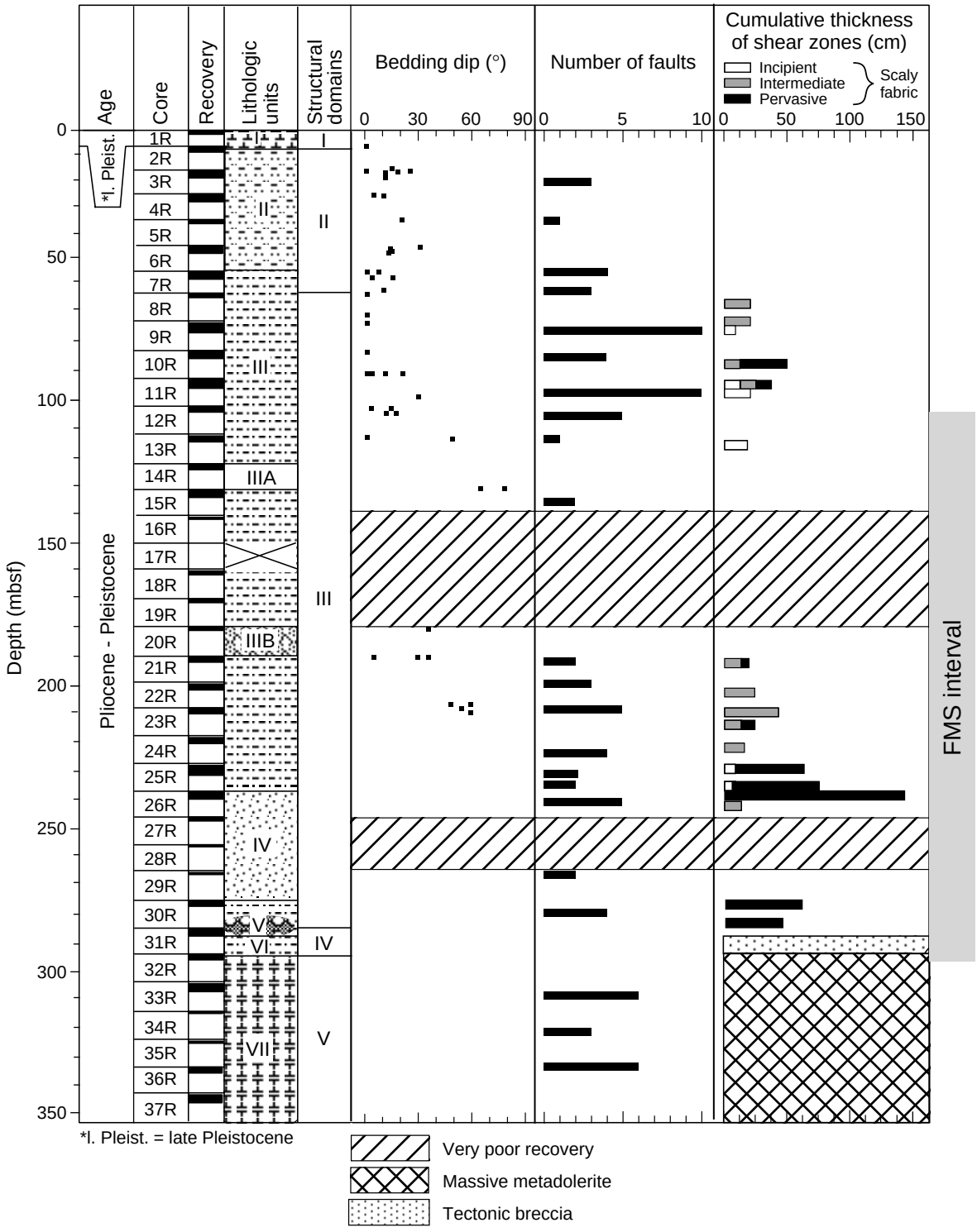

Figure F4. Composite log of Hole 1114A. Vertical scale = 1/1000. From left: (1) core, (2) core recovery, (3) depth, (4) static FMS image, (5) location of detailed FMS figures shown in this paper, (6) structural interpretation tadpoles, (7) depth intervals of fracture zone stereonets shown in this paper, (8) lithologic units, (9) logging units, (10) structural domains, and (11) caliper measurements. The thin vertical green line on the FMS images indicates the orientation of pad1, which corresponds to the C1 caliper reading. The tadpole position on the horizontal axis indicates the dip magnitude, and its tail points toward the dip direction. BRC = breccia.

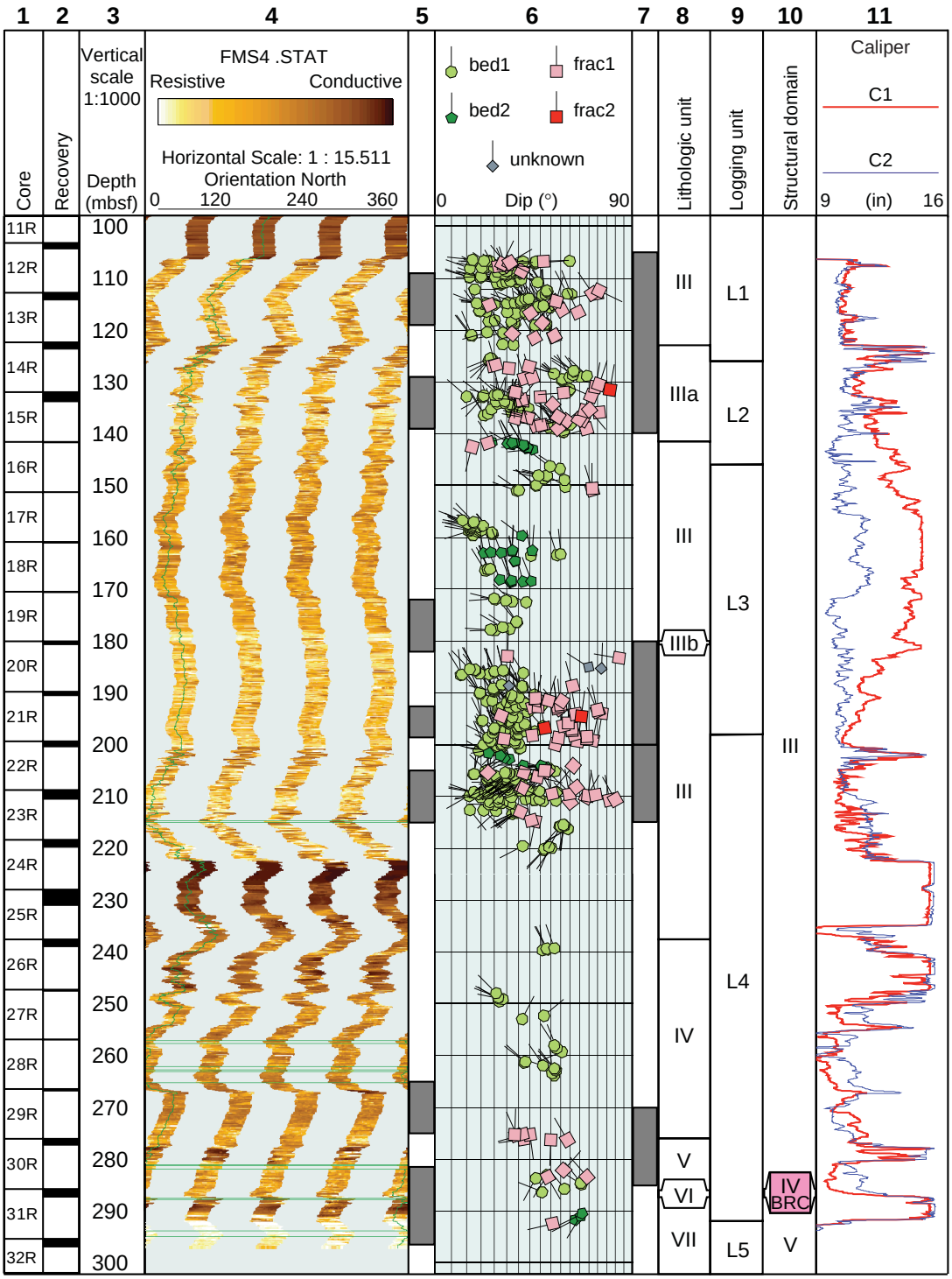

Figure F5. FMS image and analysis, 109–119 mbsf, Hole 1114A. Vertical scale = 1/40. From left: (1) depth, (2) static FMS image, (3) dynamic FMS image with a 2-m color equalization sliding window with sinusoids corresponding to the structural measurements, (4) structural interpretation tadpoles, and (5) caliper measurements. The thin vertical green line on the FMS images indicates the orientation of pad 1, which corresponds to the C1 caliper reading. The tadpole position on the horizontal axis indicates the dip magnitude, and its tail points toward the dip direction.

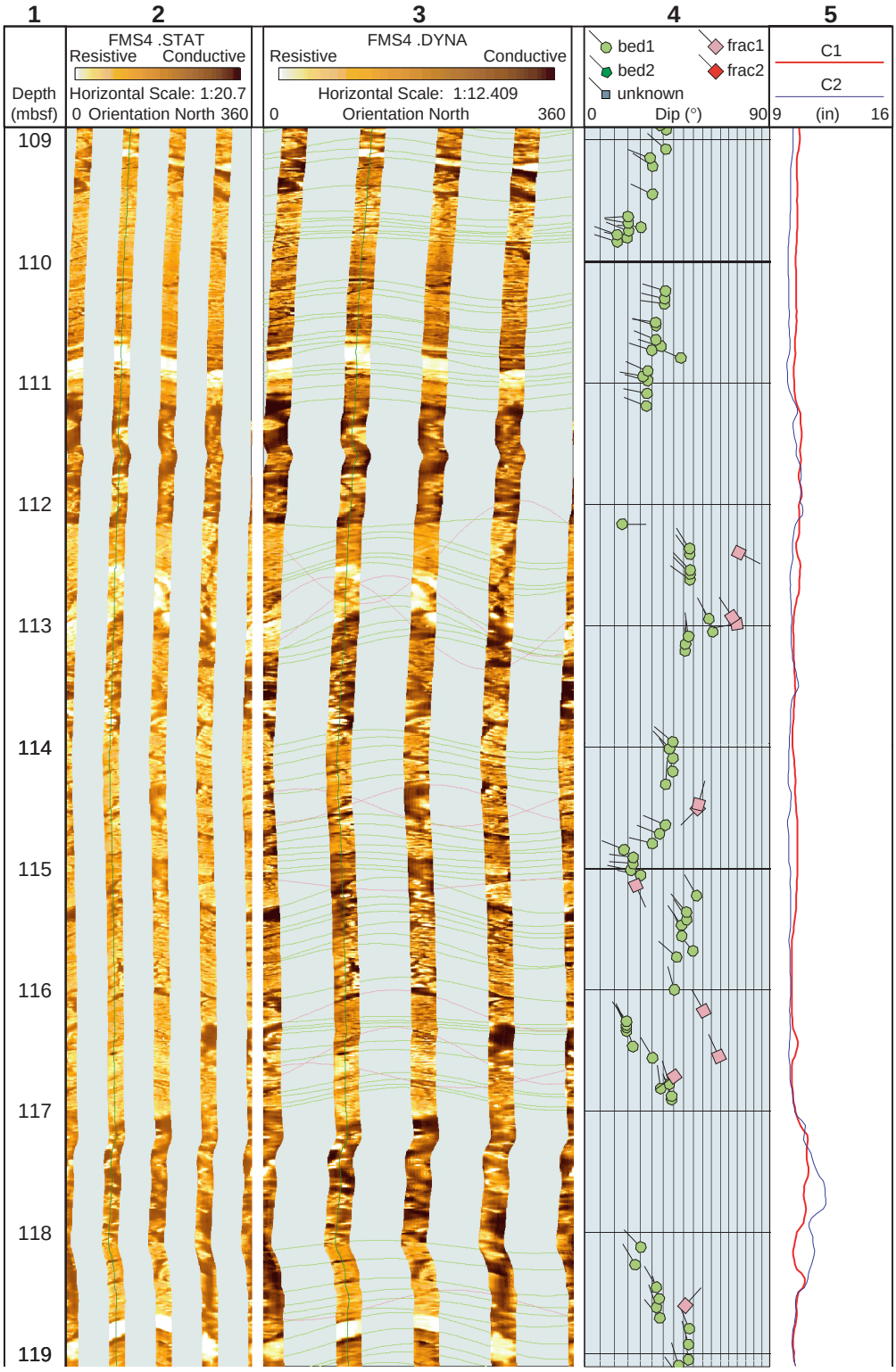

Figure F6. FMS image and analysis, 129–139 mbsf, Hole 1114A. Vertical scale = 1/40. From left: (1) depth, (2) static FMS image, (3) dynamic FMS image with a 2-m color equalization sliding window with sinusoids corresponding to the structural measurements, (4) structural interpretation tadpoles, and (5) caliper measurements. The thin vertical green line on the FMS images indicates the orientation of pad 1, which corresponds to the C1 caliper reading. The tadpole position on the horizontal axis indicates the dip magnitude, and its tail points toward the dip direction.

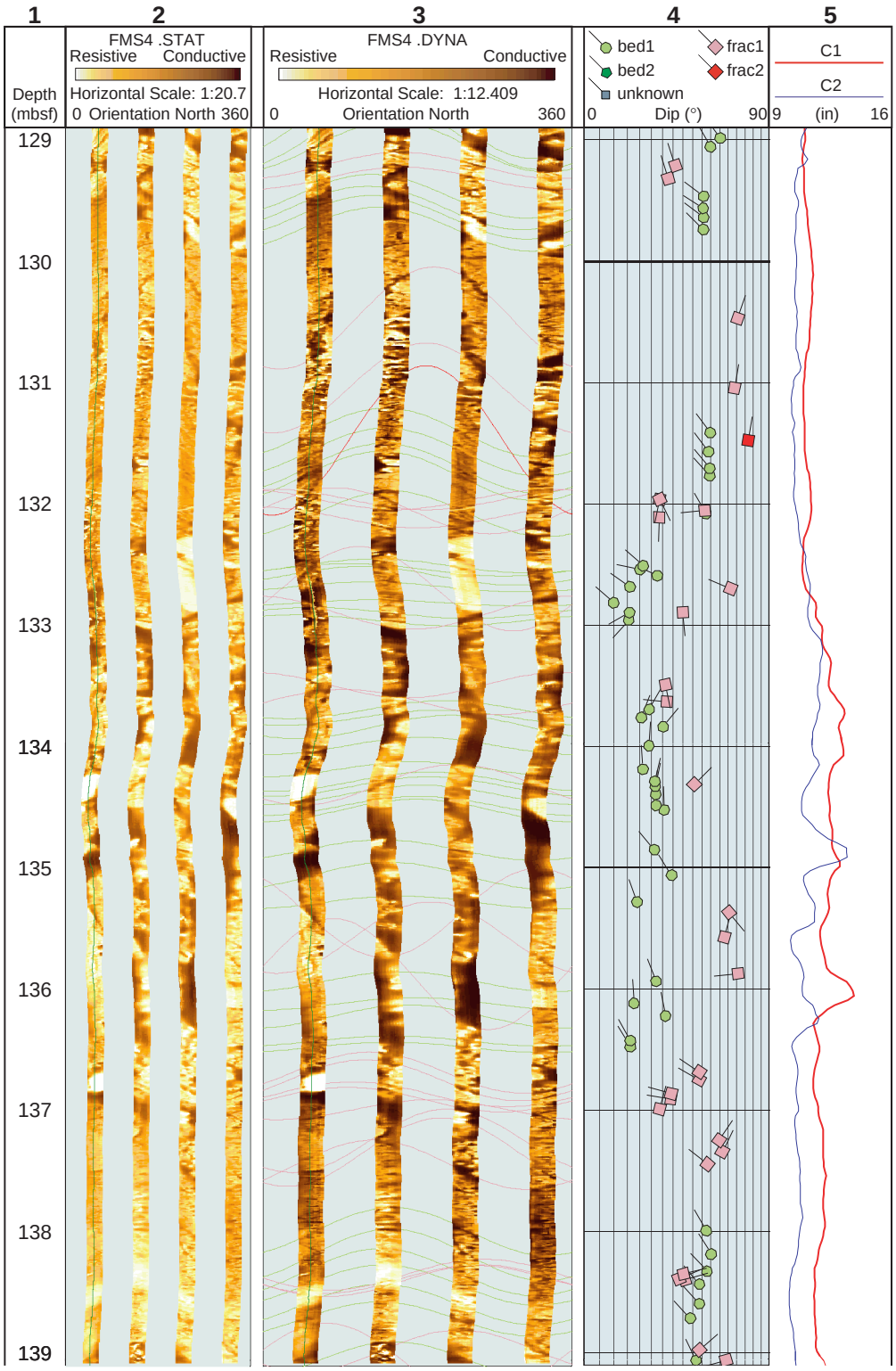

Figure F7. FMS image and analysis, 172–182 mbsf, Hole 1114A. Vertical scale = 1/40. From left: (1) depth, (2) static FMS image, (3) dynamic FMS image with a 2-m color equalization sliding window with sinusoids corresponding to the structural measurements, (4) structural interpretation tadpoles, and (5) caliper measurements. The thin vertical green line on the FMS images indicates the orientation of pad 1, which corresponds to the C1 caliper reading. The tadpole position on the horizontal axis indicates the dip magnitude, and its tail points toward the dip direction.

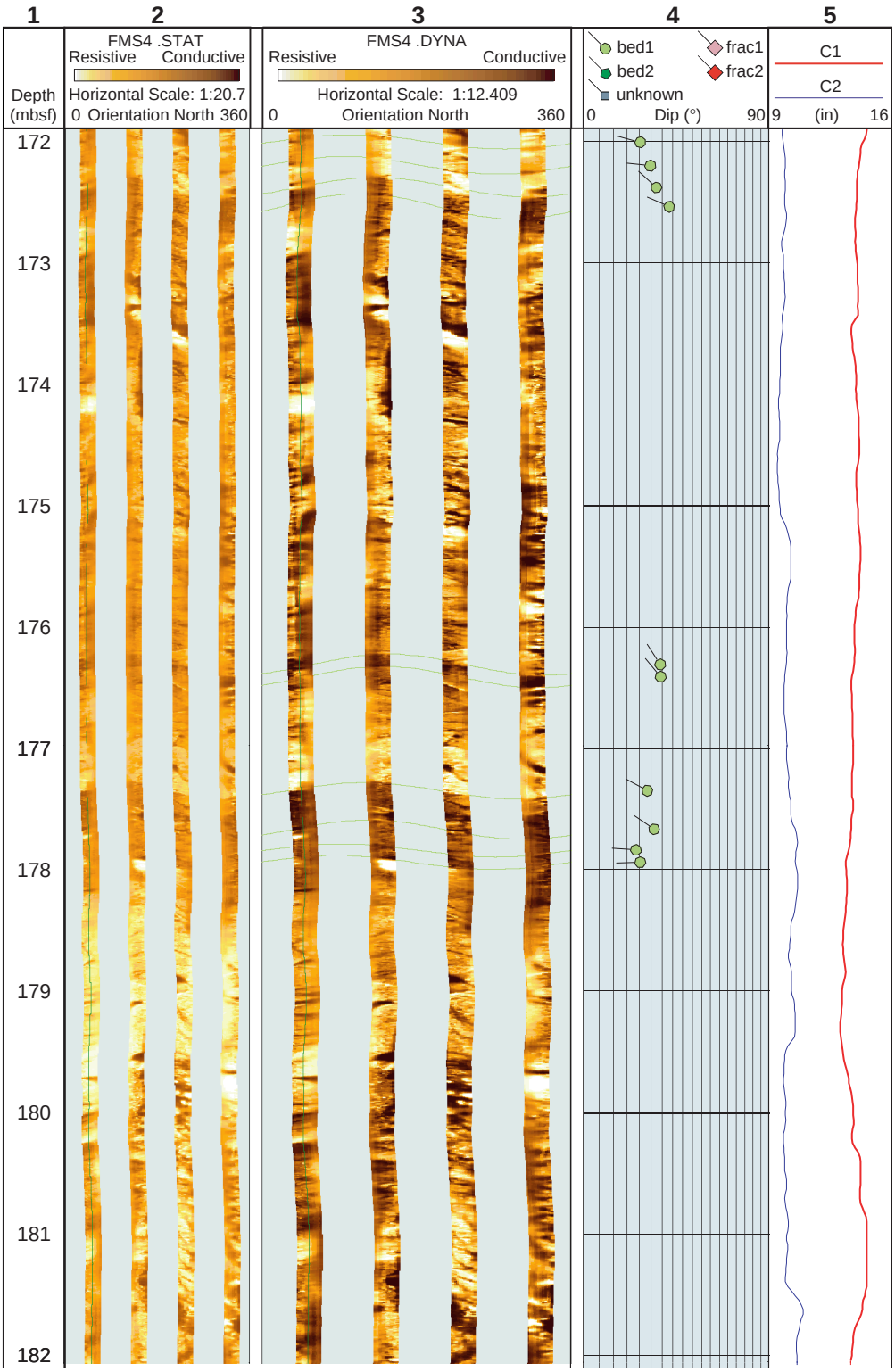

Figure F8. FMS image and analysis, 205–215 mbsf, Hole 1114A. Vertical scale = 1/40. From left: (1) depth, (2) static FMS image, (3) dynamic FMS image with a 2-m color equalization sliding window with sinusoids corresponding to the structural measurements, (4) structural interpretation tadpoles, and (5) caliper measurements. The thin vertical green line on the FMS images indicates the orientation of pad 1, which corresponds to the C1 caliper reading. The tadpole position on the horizontal axis indicates the dip magnitude, and its tail points toward the dip direction.

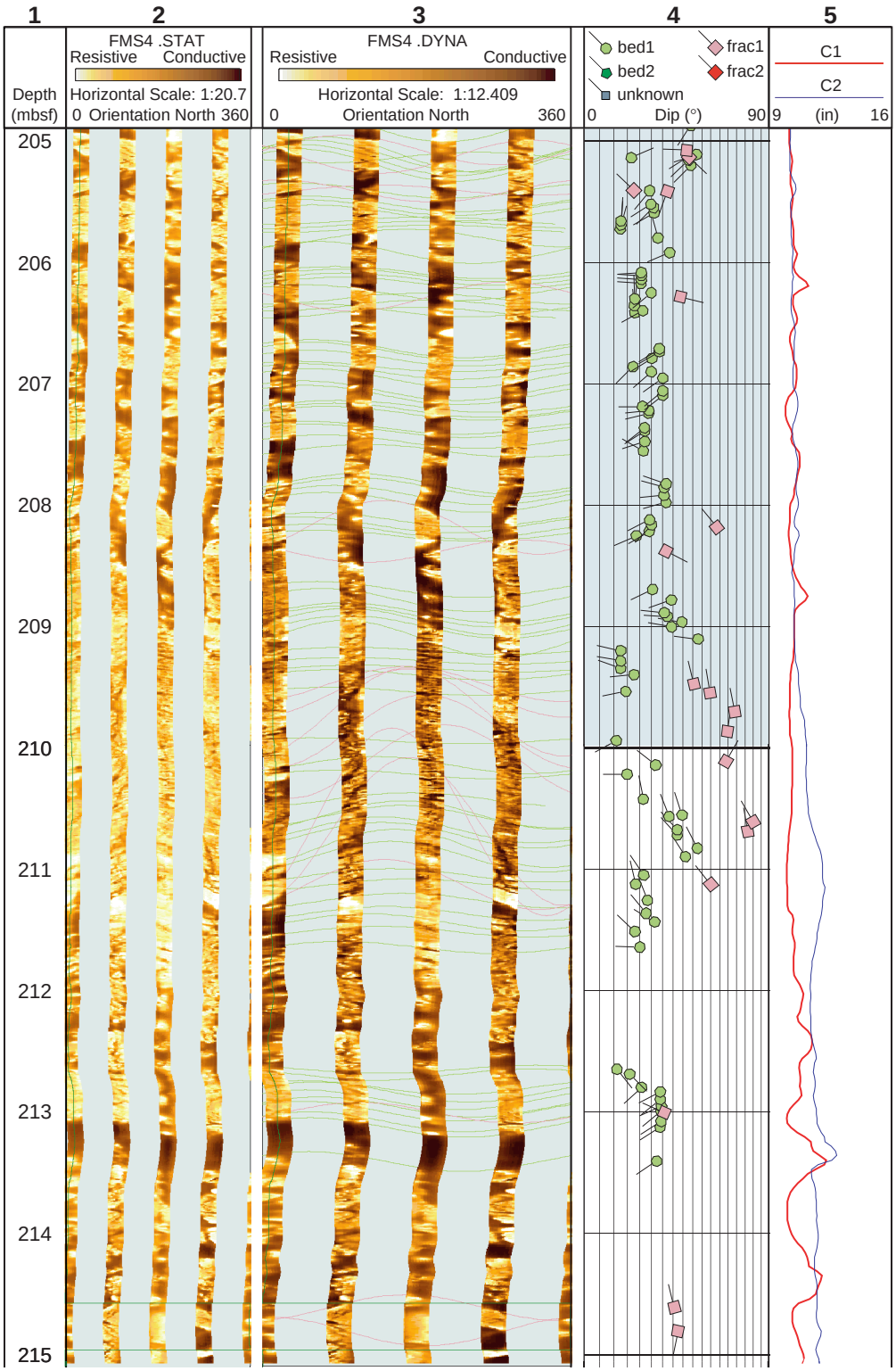

Figure F9. FMS image and analysis, 265–275 mbsf, Hole 1114A. Vertical scale = 1/40. From left: (1) depth, (2) static FMS image, (3) dynamic FMS image with a 2-m color equalization sliding window with sinusoids corresponding to the structural measurements, (4) structural interpretation tadpoles, and (5) caliper measurements. The thin vertical green line on the FMS images indicates the orientation of pad 1, which corresponds to the C1 caliper reading. The tadpole position on the horizontal axis indicates the dip magnitude, and its tail points toward the dip direction.

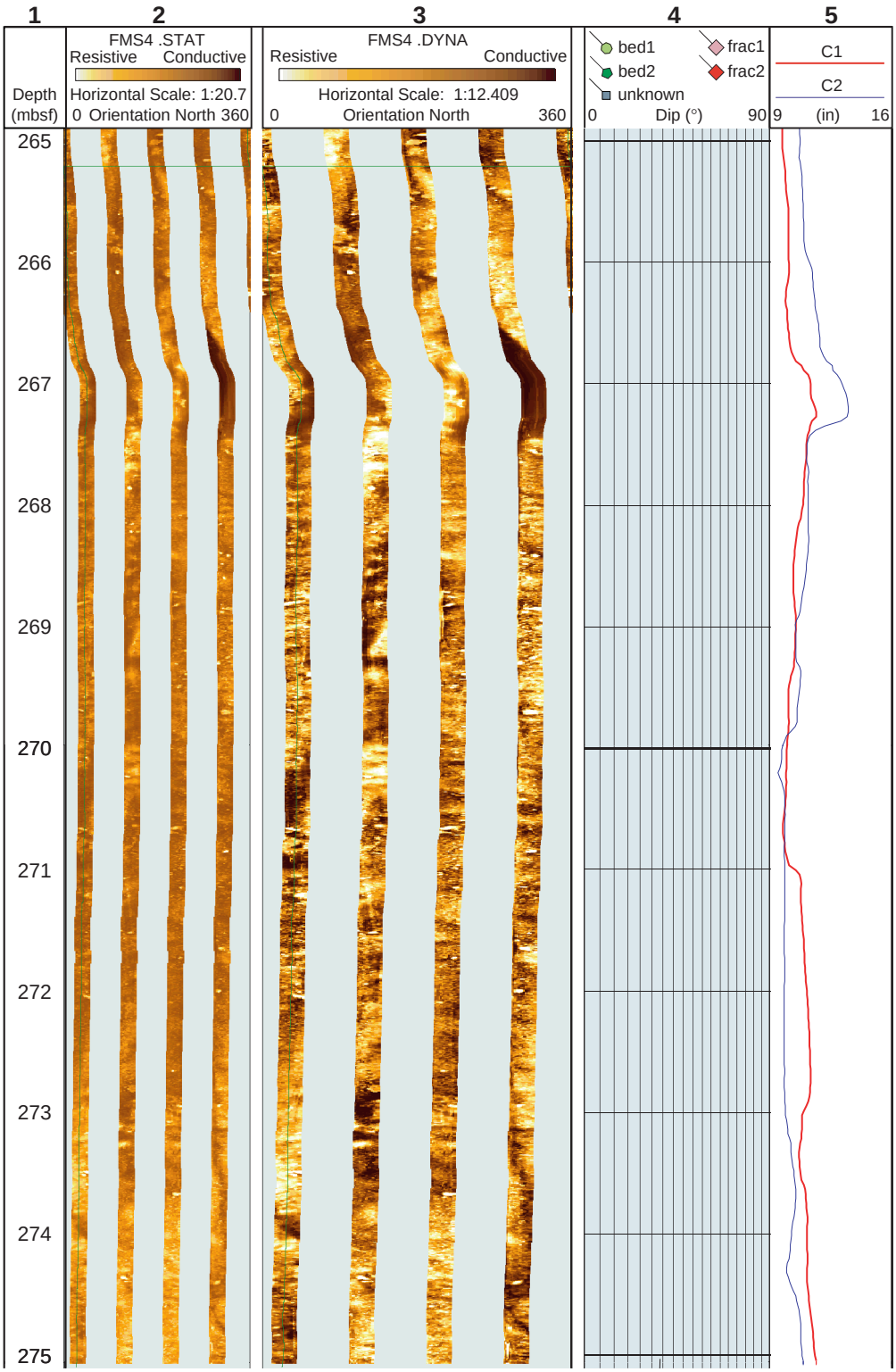

Figure F10. FMS image and analysis, 282–296 mbsf, Hole 1114A. Vertical scale = 1/40.From left: (1) depth, (2) static FMS image, (3) dynamic FMS image with a 2-m color equalization sliding window with sinusoids corresponding to the structural measurements, (4) structural interpretation tadpoles, and (5) caliper measurements. The thin vertical green line on the FMS images indicates the orientation of pad 1, which corresponds to the C1 caliper reading. The tadpole position on the horizontal axis indicates the dip magnitude, and its tail points toward the dip direction. Note the sediment /tectonic breccia contact at 291 mbsf.

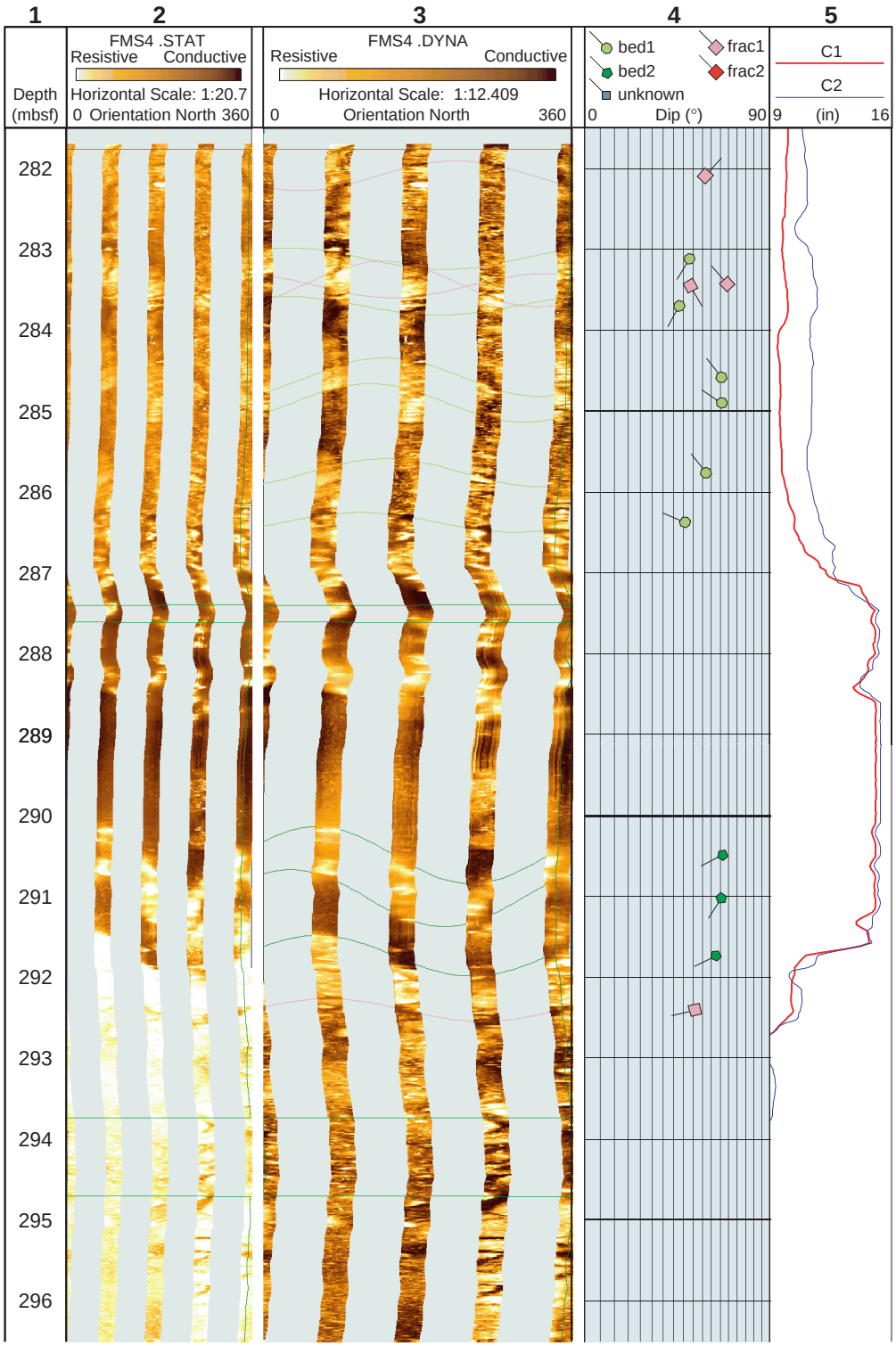

Figure F11. Hole 1114A global bed orientations. Equal area stereographic projection, lower hemisphere. Poles to bed 1 and bed 2 are shown as light green circles and darker green pentagons, respectively. Strike and dip histograms use 5° bins. Strike is normalized so that the dip direction is 90° clockwise from strike. Bed 1 and bed 2 histograms are stacked with the same color code as stereonet poles.

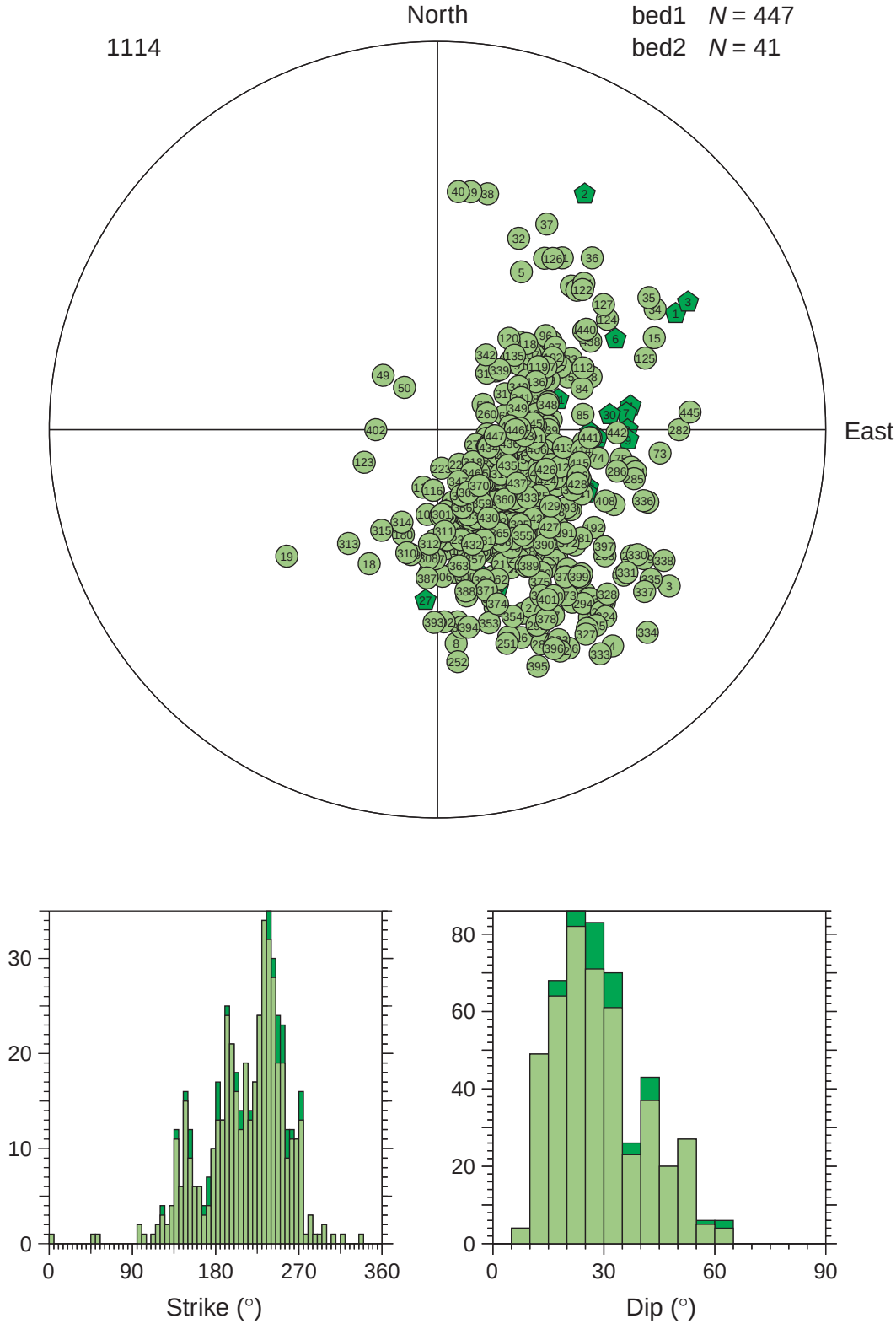

Figure F12. Hole 1114A global fracture orientations. Equal area stereographic projection, lower hemisphere. Poles to frac 1 and frac 2 are shown as pink and red squares, respectively. Strike and dip histograms use 5° bins. Strike is normalized so that the dip direction is 90° clockwise from strike. Frac 1 and frac 2 histograms are stacked with the same color code as stereonet poles.

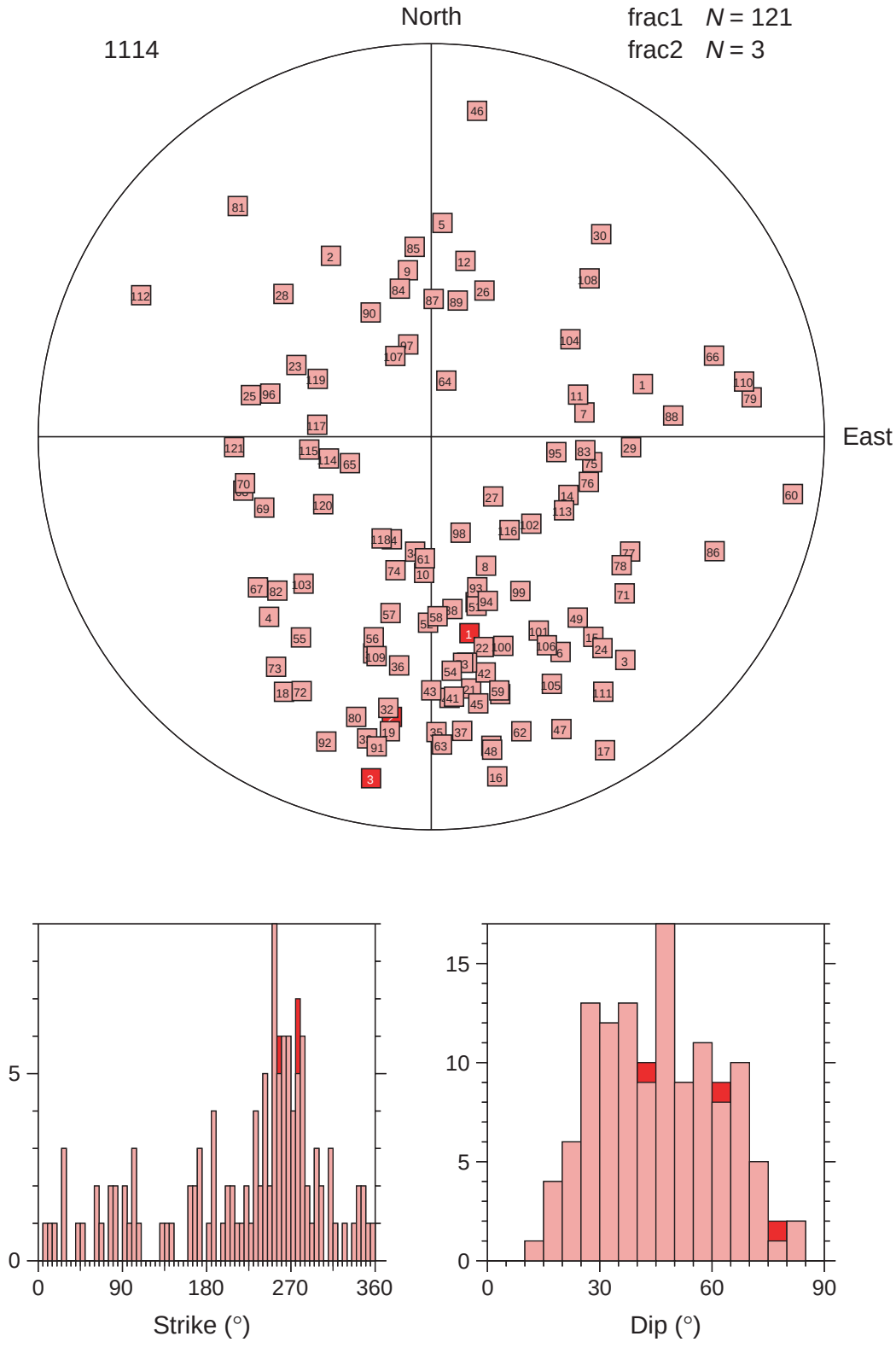

Figure F13. Hole 1114A global unknown planar structure orientations. Equal area stereographic projection, lower hemisphere. Poles are shown as gray diamonds. Strike and dip histograms use 5° bins. Strike is normalized so that the dip direction is 90° clockwise from strike.

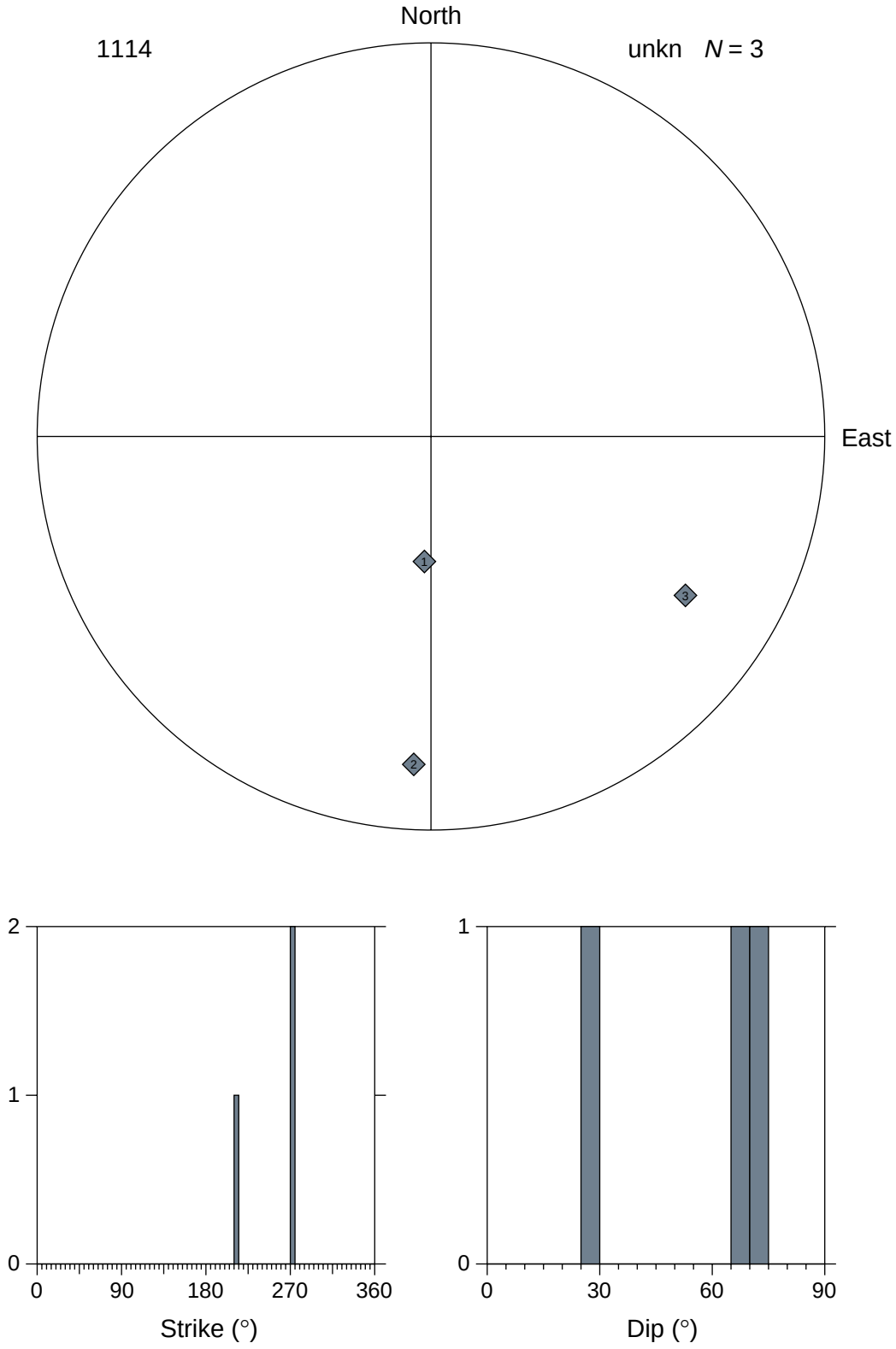

Figure F14. Fracture dip, dip direction, and density vs. depth (number of fractures per meter) from FMS images analysis at Hole 1114A. Black squares = fractures, open diamonds = reverse faults. The line at 200 mbsf shows the sharp change of fracture dip direction within FZ2, which is therefore subdivided into FZ2a and FZ2b.

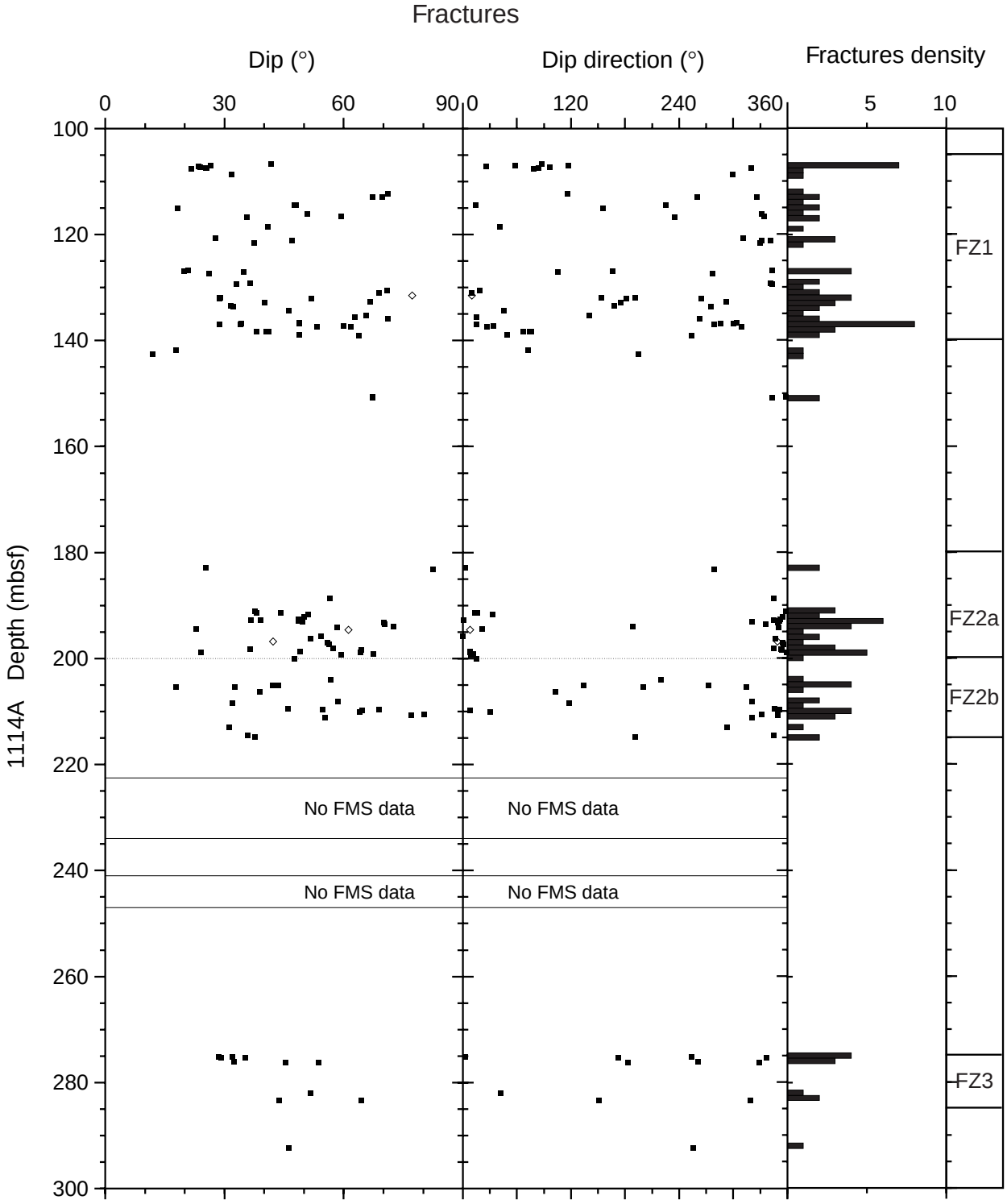

Figure F15. Hole 1114A FZ1 fracture orientations. Poles to frac 1 and frac 2 are shown as pink and red squares, respectively. Strike and dip histograms use 5° bins. Strike is normalized so that the dip direction is 90° clockwise from strike. Frac 1 and frac 2 histograms are stacked with the same color code as stereonet poles.

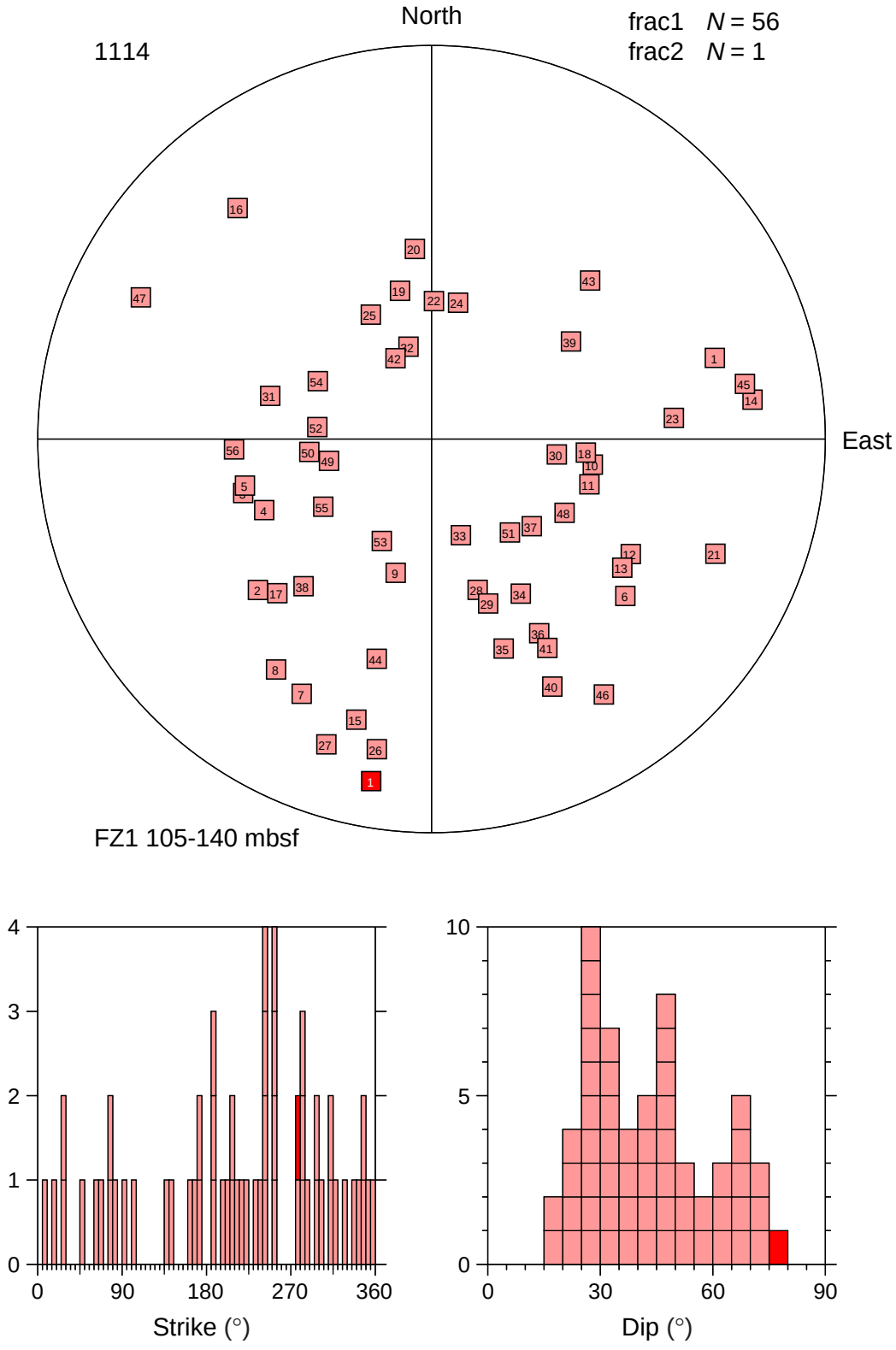

Figure F16. Hole 1114A FZ2 fracture orientations. Poles to frac 1 and frac 2 are shown as pink and red squares, respectively. Strike and dip histograms use 5° bins. Strike is normalized so that the dip direction is 90° clockwise from strike. Frac 1 and frac 2 histograms are stacked with the same color code as stereonet poles.

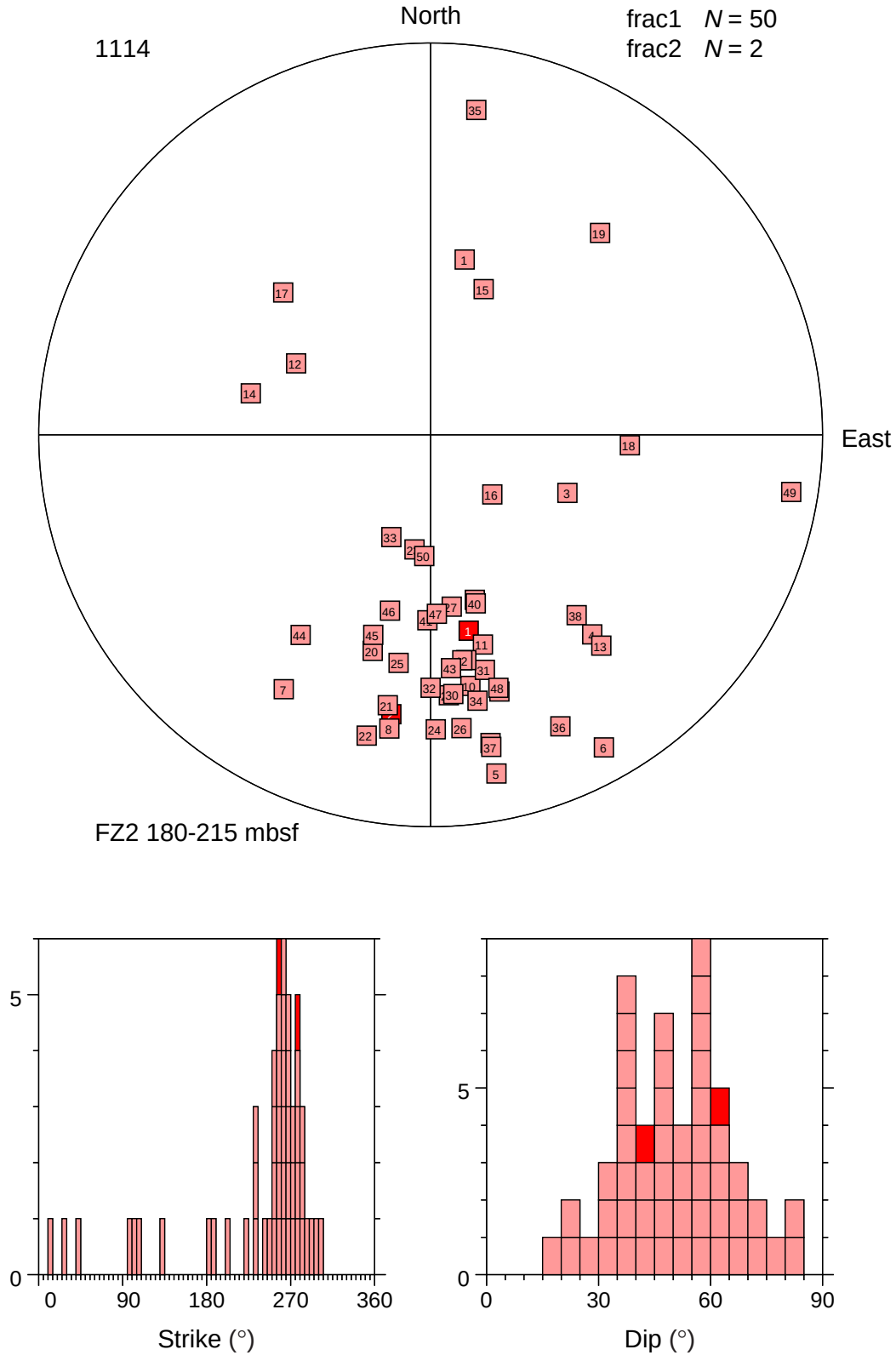

Figure F17. Hole 1114A FZ3 fracture orientations. Poles to frac 1 and frac 2 are shown as pink and red squares, respectively. Strike and dip histograms use 5° bins. Strike is normalized so that the dip direction is 90° clockwise from strike. Frac 1 and frac 2 histograms are stacked with the same color code as stereonet poles.

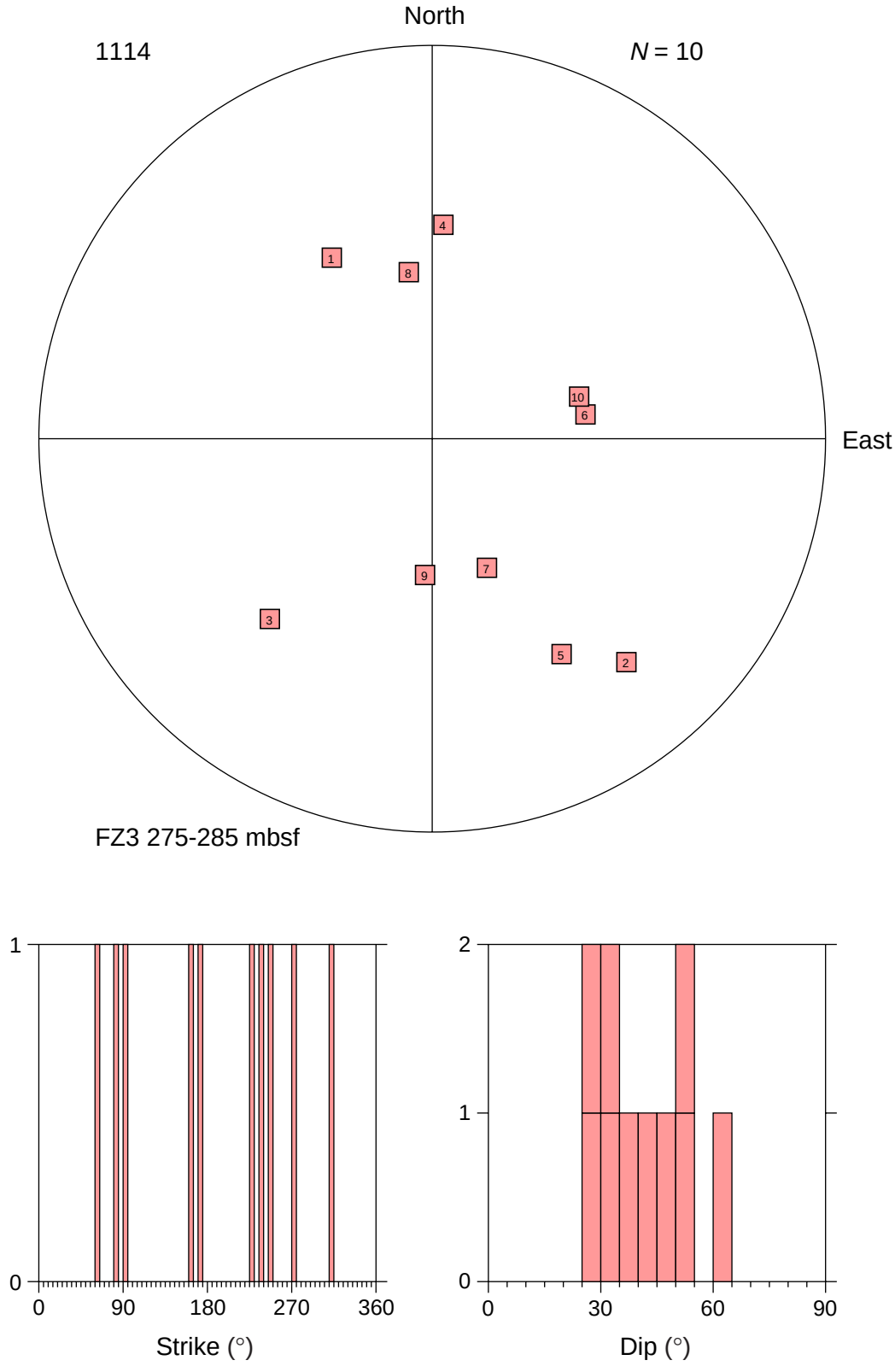

Figure F18. Hole 1114A FZ2a fracture orientations. Poles to frac 1 and frac 2 are shown as pink and red squares, respectively. Strike and dip histograms use 5° bins. Strike is normalized so that the dip direction is 90° clockwise from strike. Frac 1 and frac 2 histograms are stacked with the same color code as stereonet poles.

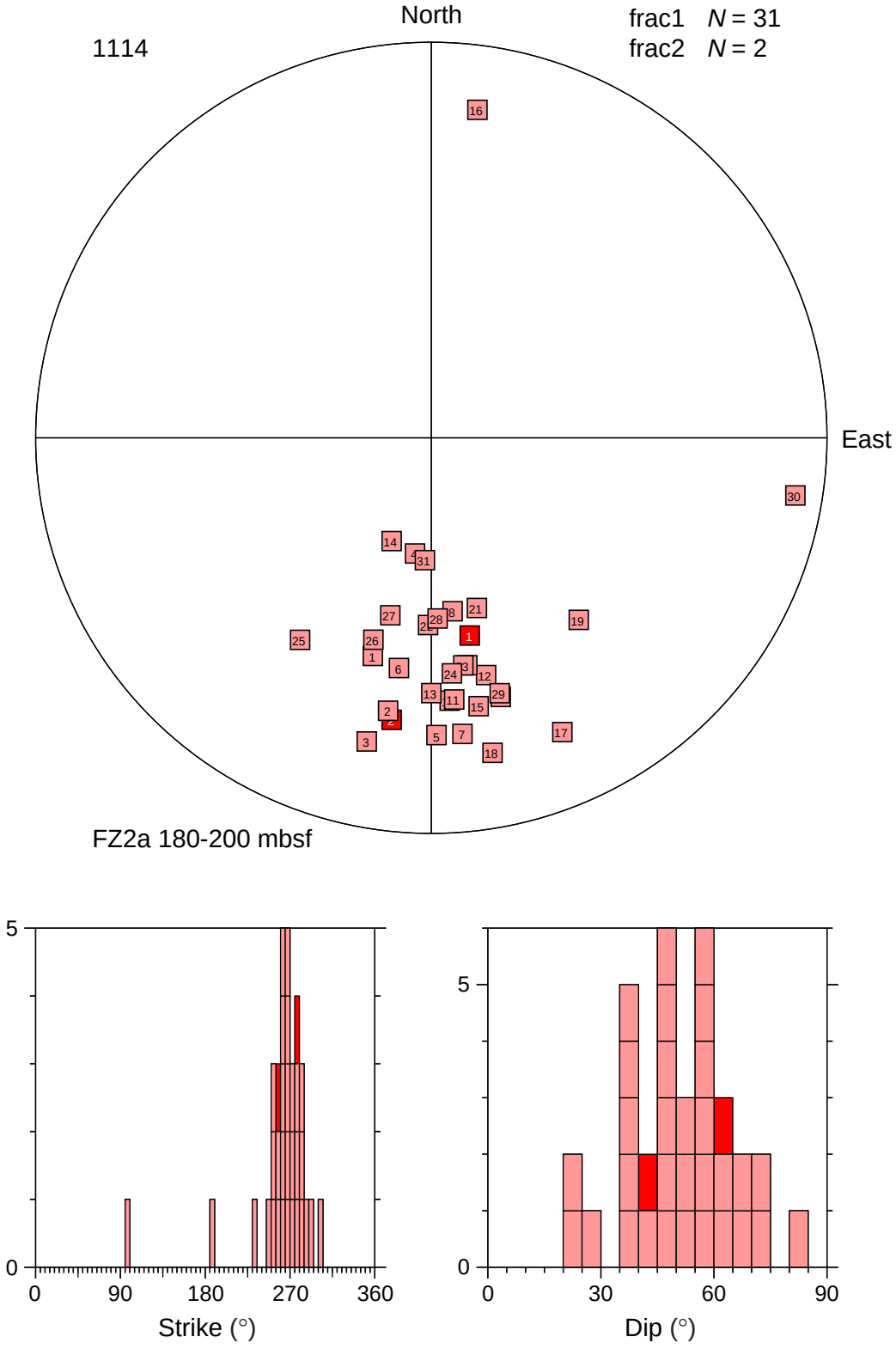

Figure F19. Hole 1114A FZ2b fracture orientations. Poles to frac 1 and frac 2 are shown as pink and red squares, respectively. Strike and dip histograms use 5° bins. Strike is normalized so that the dip direction is 90° clockwise from strike. Frac 1 and frac 2 histograms are stacked with the same color code as stereonet poles.

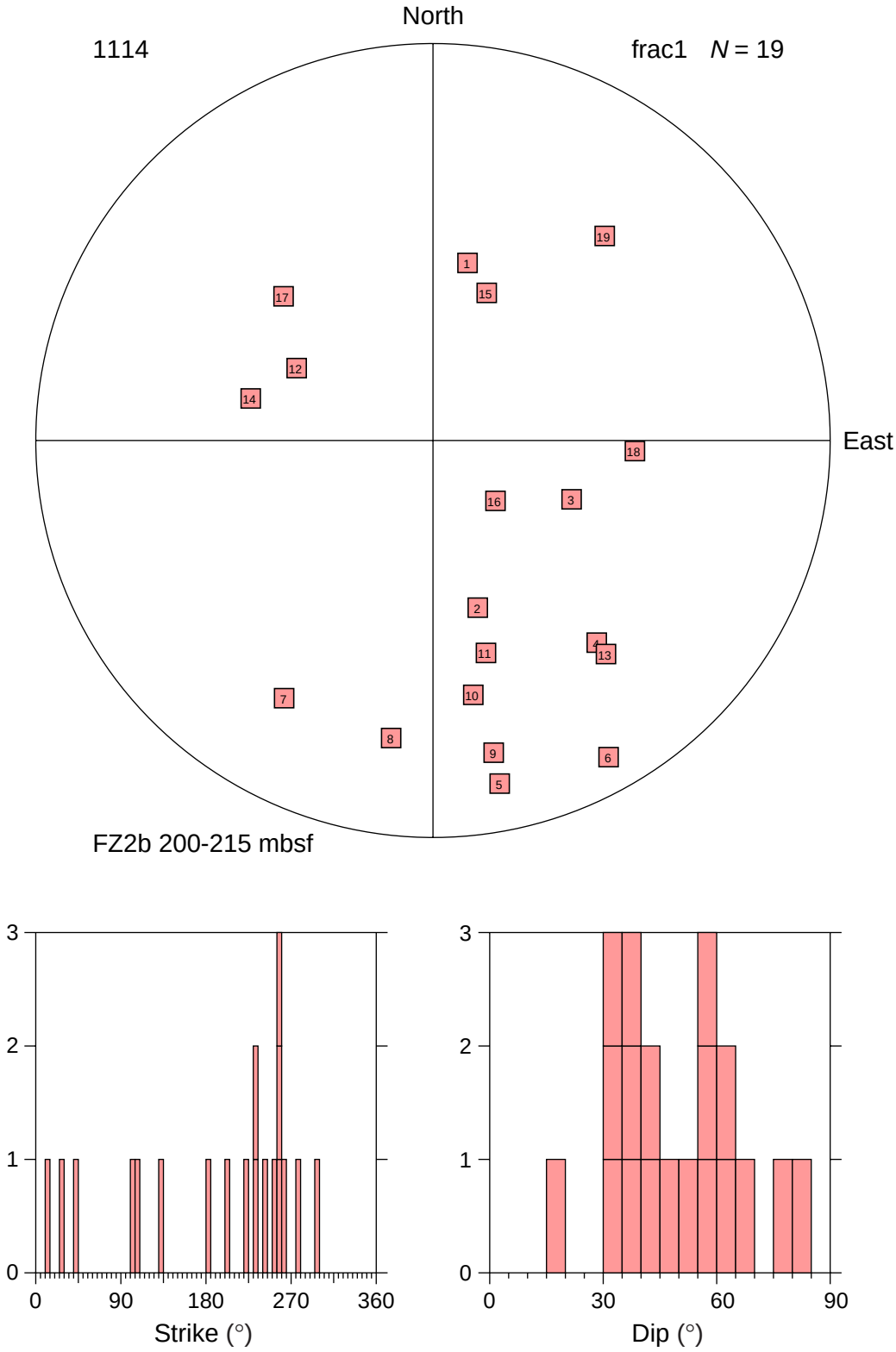

Figure F20. Close up of a reverse fault (orange sinusoid) in FZ1. A small reverse offset of thin resistive layers is observed on pads 1, 3, and 4, from left. An array of microreverse faults was also observed in a core at the same depth (core photograph is from Shipboard Scientific Party, 1999c).

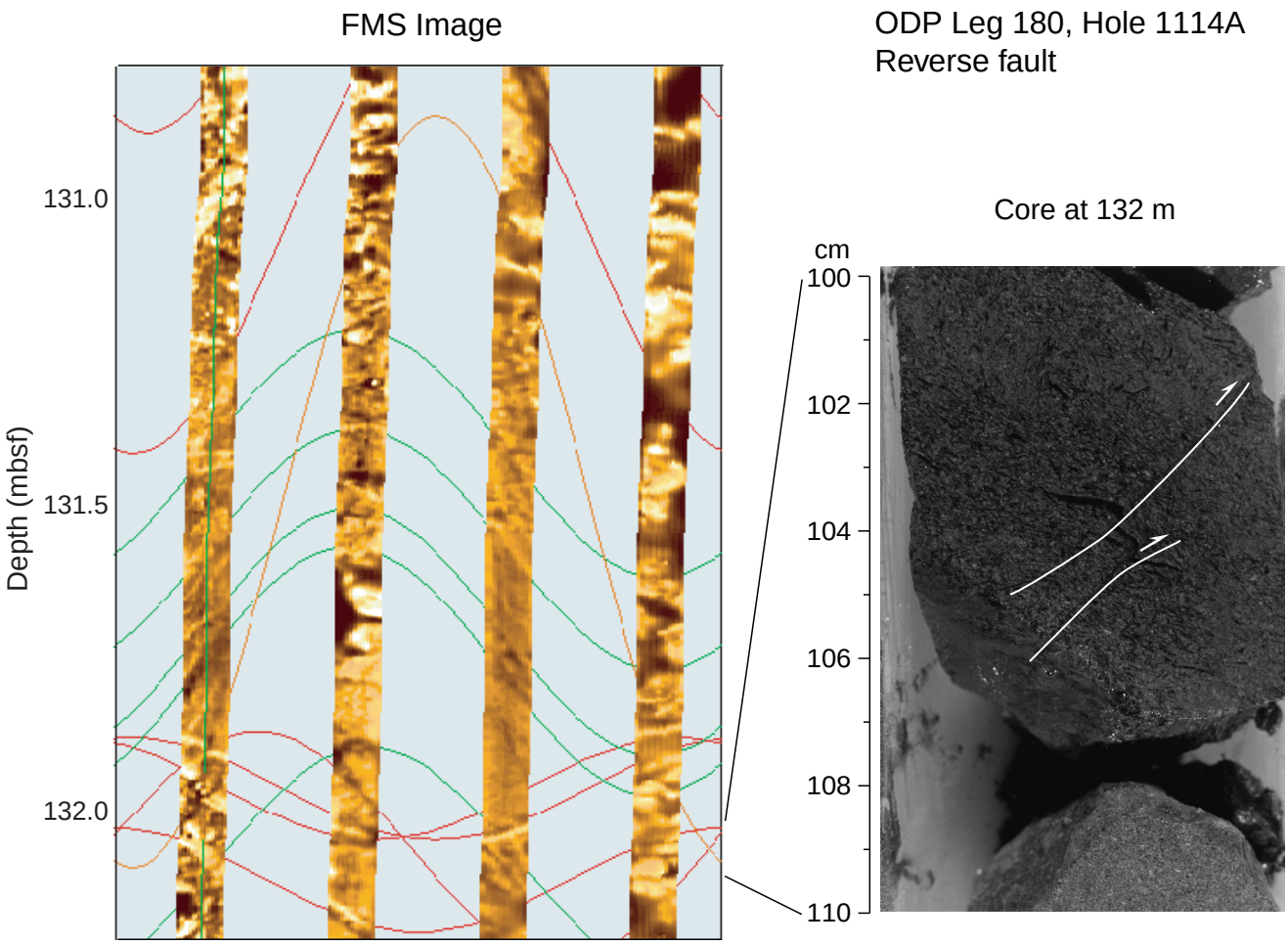

Figure F21. Close up of two reverse faults in FZ2. From left: (1) depth, (2) static FMS image, (3) dynamic FMS image with a 2-m color equalization sliding window with sinusoids corresponding to the structural measurements, (4) structural interpretation tadpoles, and (5) caliper measurements. The thin vertical green line on the FMS images indicates the orientation of pad 1, which corresponds to the C1 caliper reading. The tadpole position on the horizontal axis indicates the dip magnitude, and its tail points toward the dip direction. A 10-cm-thick resistive bed is cut and shifted by the upper reverse fault.

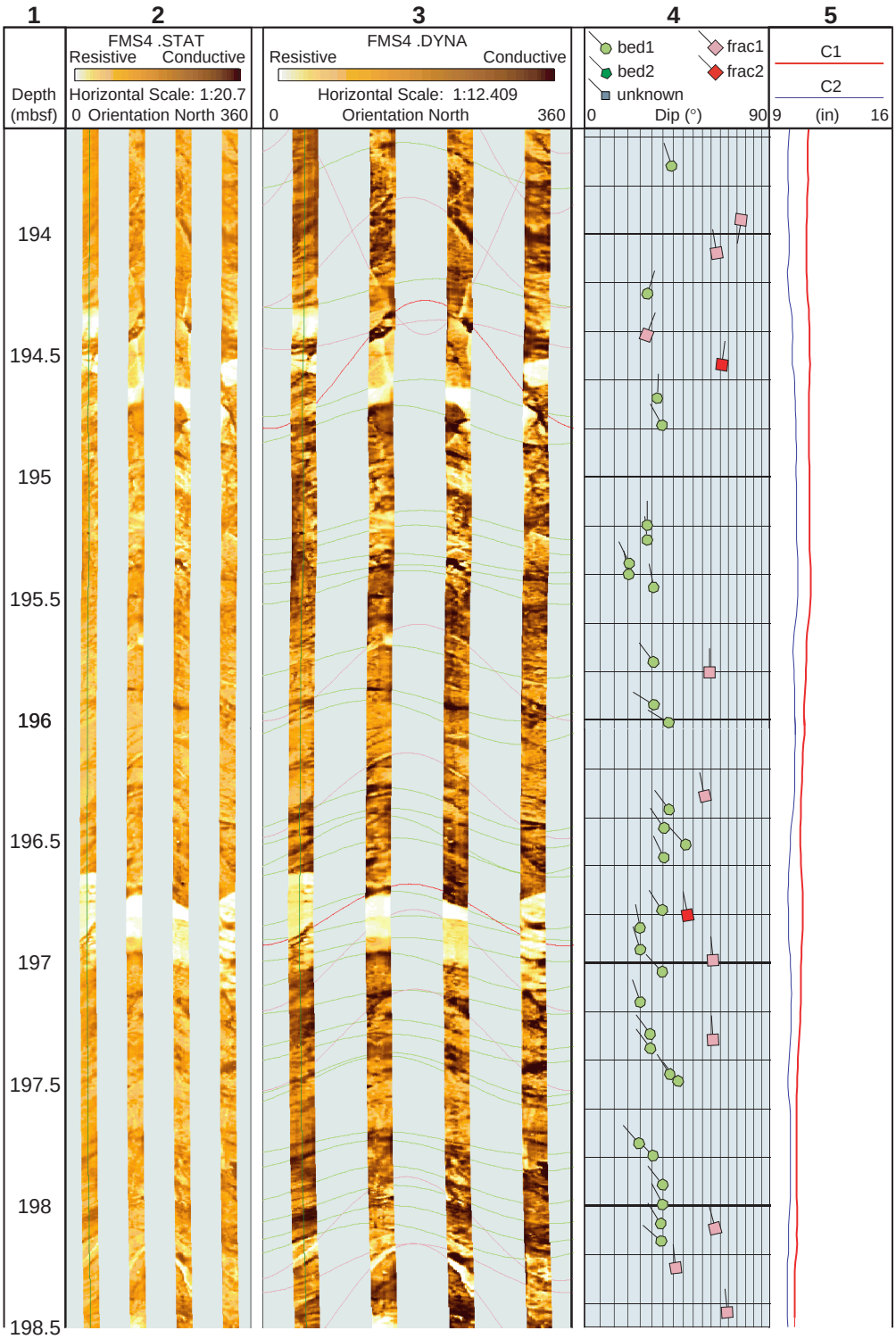

Figure F22. Bedding dip and dip direction vs. depth from FMS images analysis in Hole 1114A. Four intervals (B1–B4) are defined. The 200-m-deep line shows the sharp change of bedding dip direction between B2 and B3.

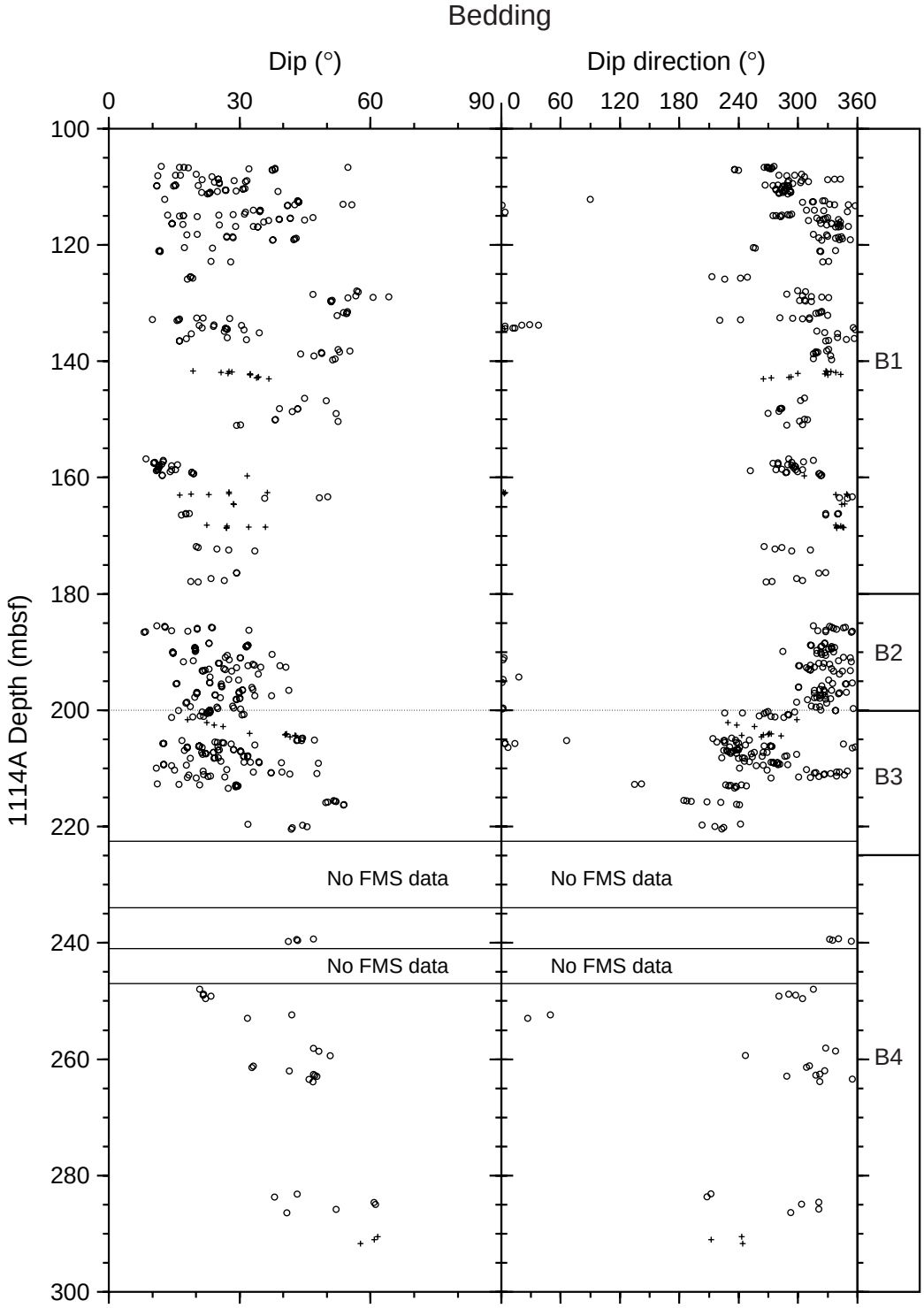

Figure F23. Hole 1114A B1 bedding orientations. Poles to bed 1 and bed 2 are shown as light green circles and darker green pentagons, respectively. Strike and dip histograms use 5° bins. Strike is normalized so that the dip direction is 90° clockwise from strike. Bed 1 and bed 2 histograms are stacked with the same color code as stereonet poles.

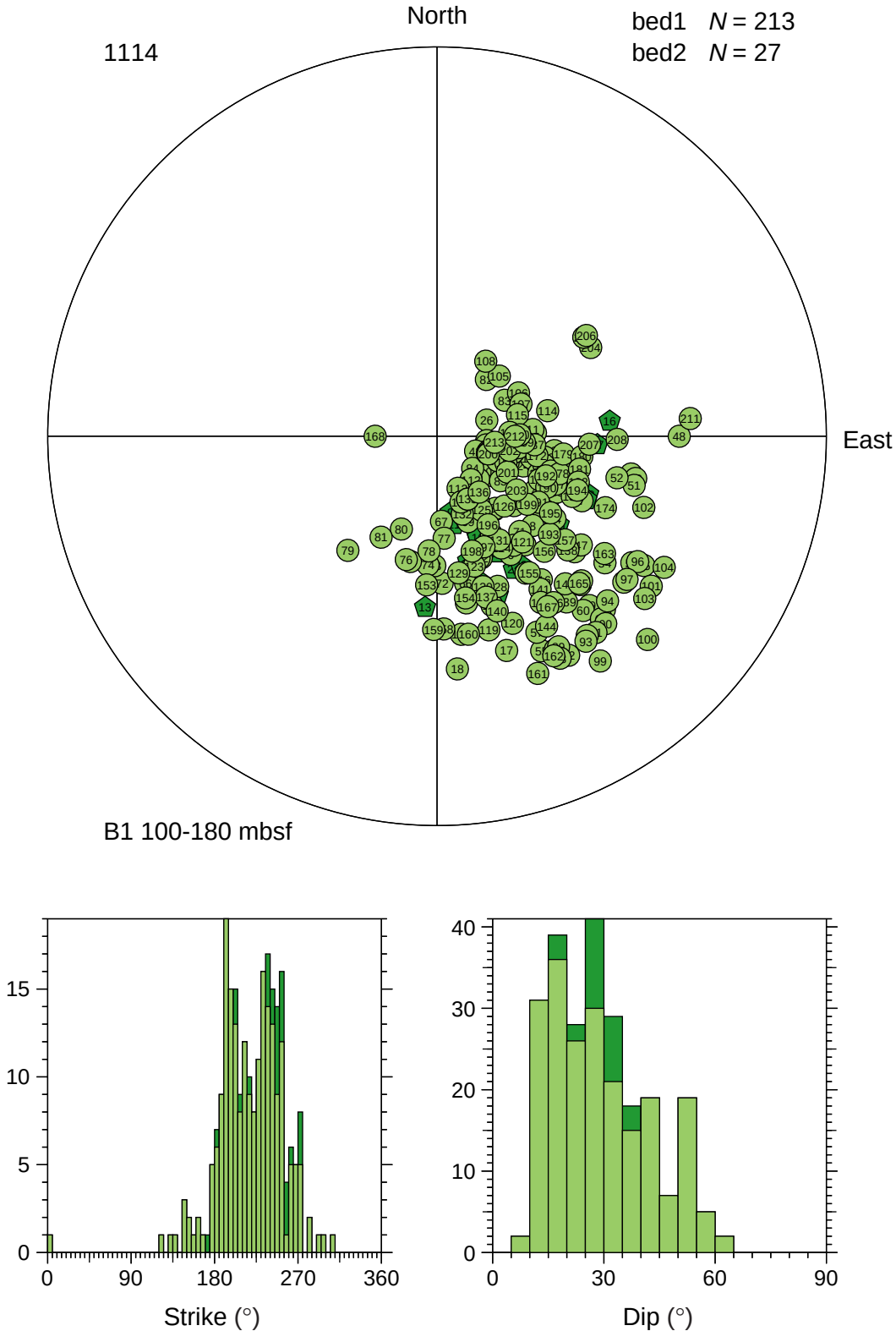

Figure F24. Hole 1114A B2 bedding orientations. Poles to bed 1 and bed 2 are shown as light green circles and darker green pentagons, respectively. Strike and dip histograms use 5° bins. Strike is normalized so that the dip direction is 90° clockwise from strike. Bed 1 and bed 2 histograms are stacked with the same color code as stereonet poles.

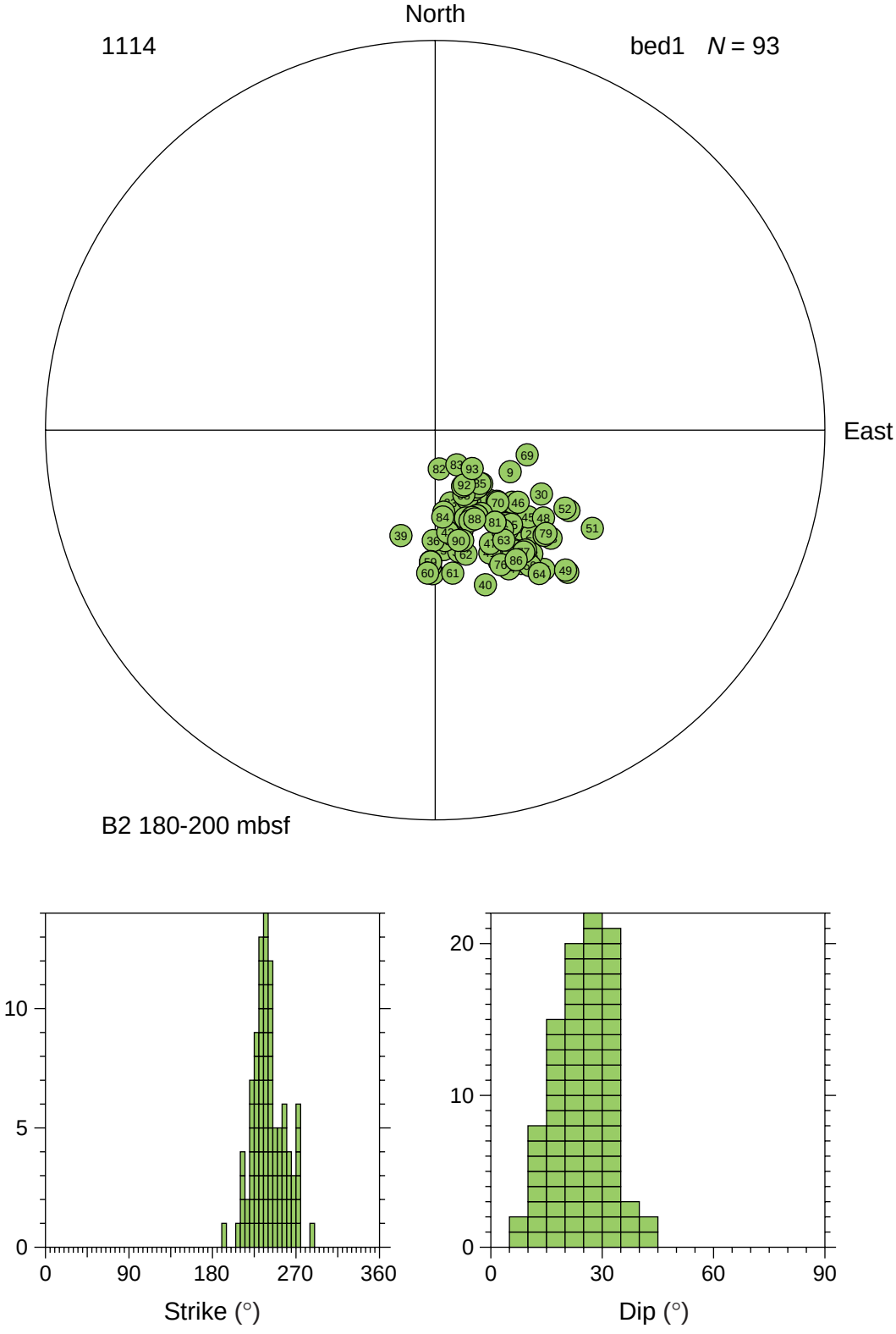

Figure F25. Hole 1114A B3 bedding orientations. Poles to bed 1 and bed 2 are shown as light green circles and darker green pentagons, respectively. Strike and dip histograms use 5° bins. Strike is normalized so that the dip direction is 90° clockwise from strike. Bed 1 and bed 2 histograms are stacked with the same color code as stereonet poles.

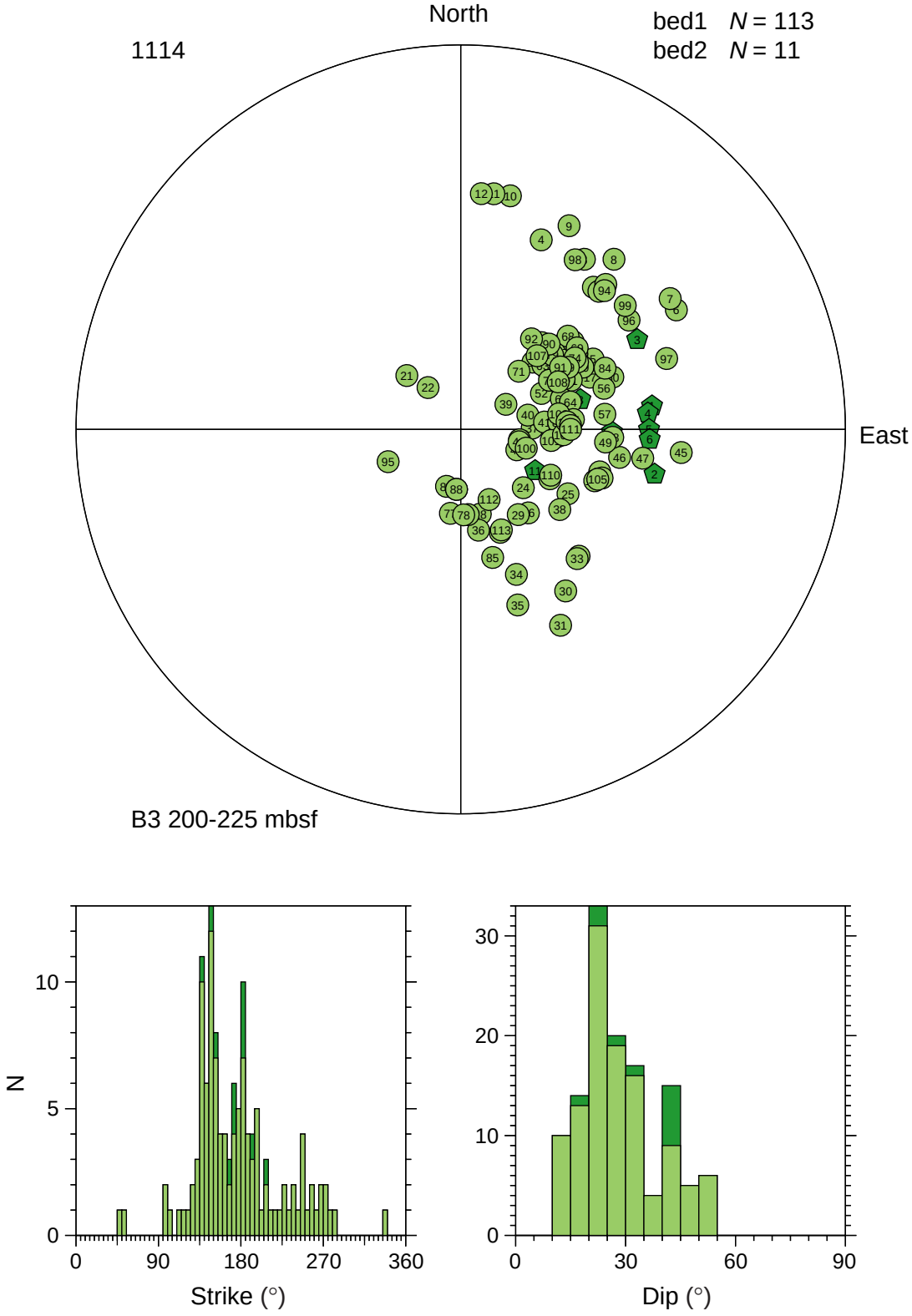

Figure F26. Hole 1114A B4 bedding orientations. Poles to bed 1 and bed 2 are shown as light green circles and darker green pentagons, respectively. Strike and dip histograms use 5° bins. Strike is normalized so that the dip direction is 90° clockwise from strike. Bed 1 and bed 2 histograms are stacked with the same color code as stereonet poles.

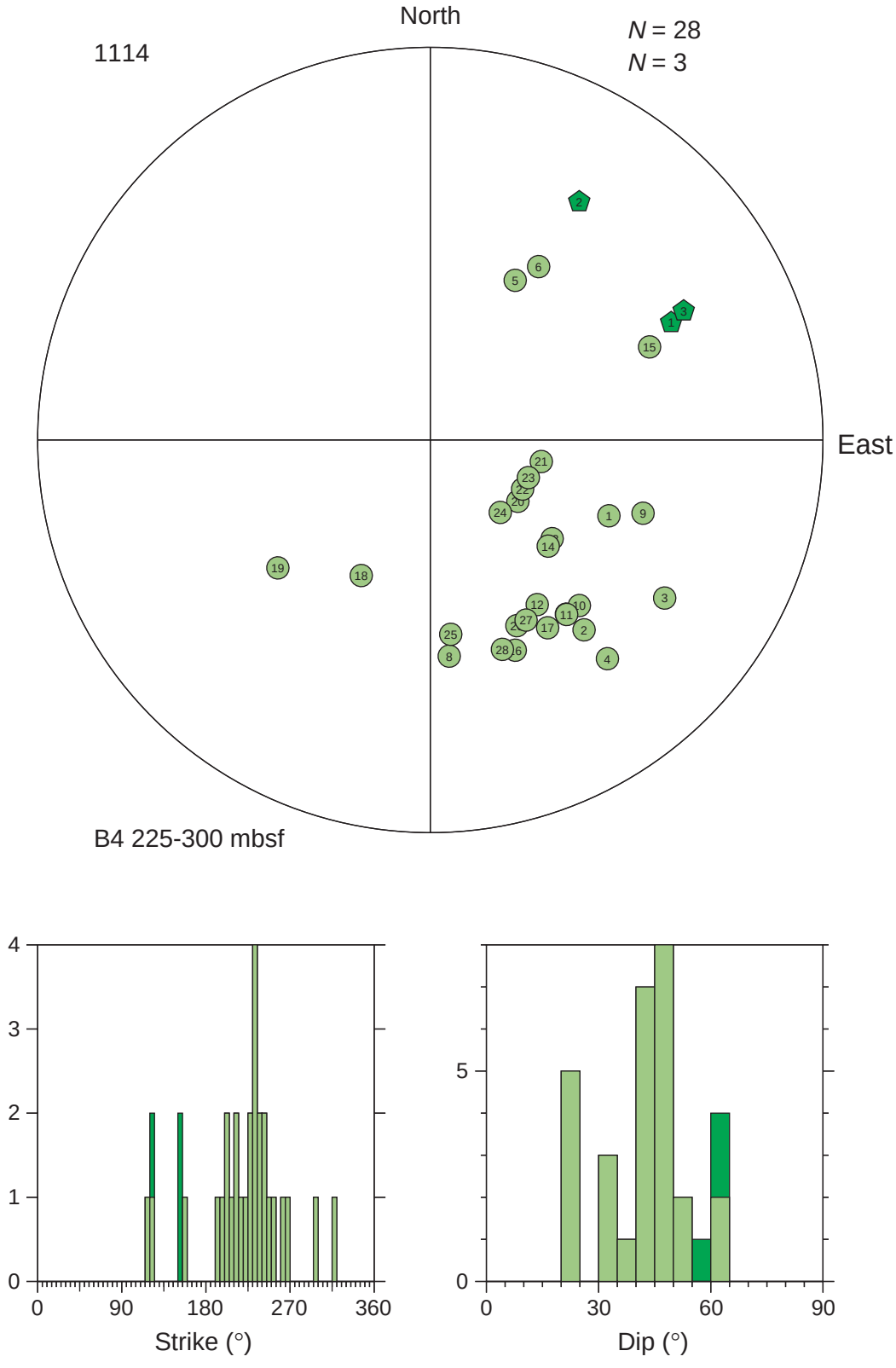

Figure F27. Interpretative structural log for Site 1114 from core and FMS image analysis.

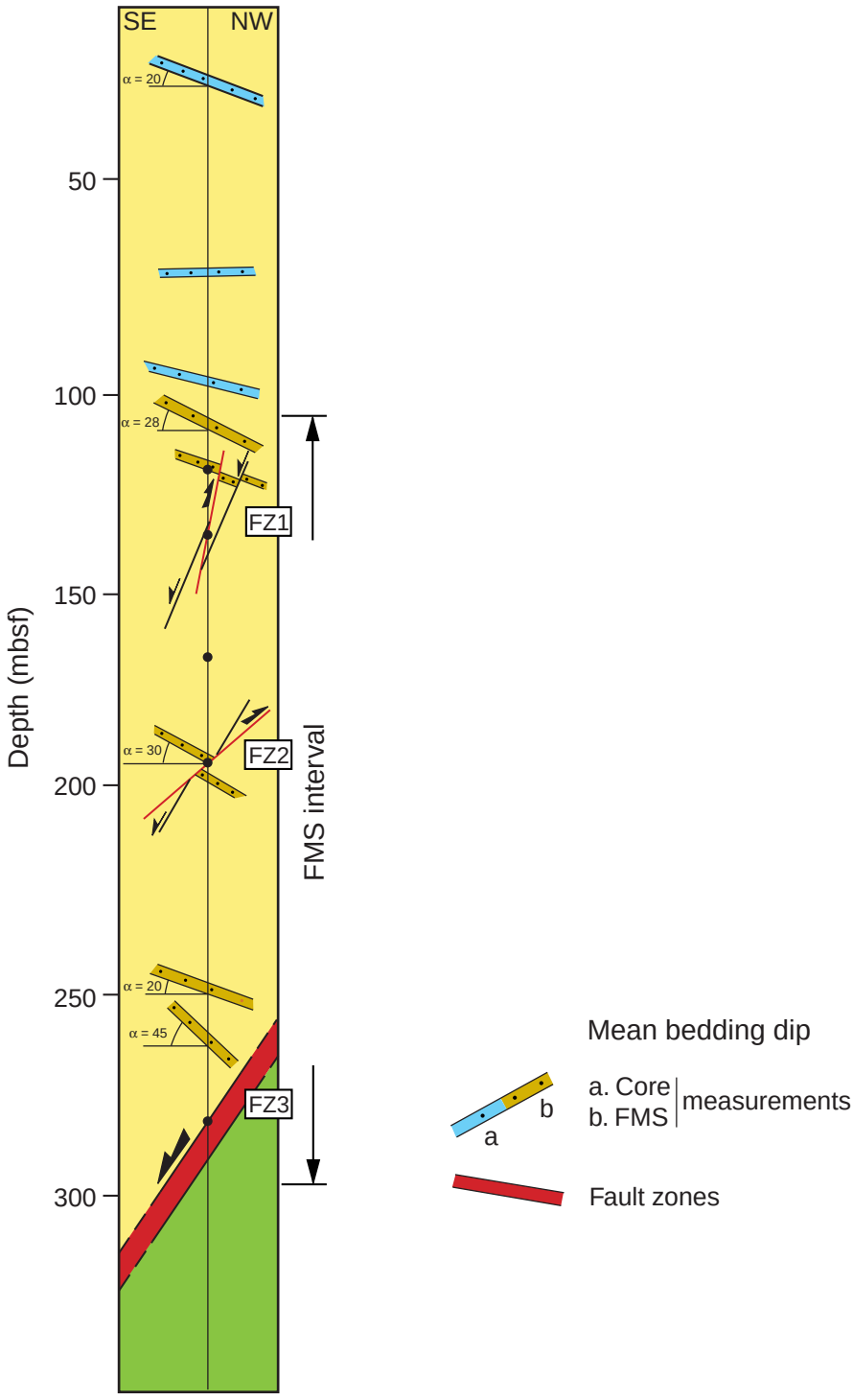

Table T1. Hole 1114A interpreted FMS images.

Figure	Depth (mbsf)	Depth scale	Lithologic unit	Logging unit	Comments
F4, p. 15	100–300	1/1000	III–VII	L1–L5	Full hole view
AF1, p. 40	100–150	1/200	III	L1–L3	
AF1, p. 40	150–200	1/200	III	L3–L4	
AF1, p. 40	200–250	1/200	III–IV	L4	
AF1, p. 40	250–300	1/200	IV–VII	L4–L5	
F5, p. 16	109–119	1/40	III	L1	Sharp resistive beds
F6, p. 17	129–139	1/40	IIIA	L2	Fracture zone
F7, p. 18	172–182	1/40	III, IIIB	L3	Conglomerate and sandstone
F21, p. 32	196.5–198.5	1/20	III	L3	Fracture zone 2
F8, p. 19	205–215	1/40	III	L4	Fracture zone 2
F9, p. 20	265–275	1/40	IV	L4	Sandstone
F10, p. 21	281.5–296.5	1/60	VI, VII	L4, L5	Sediment/breccia contact

Figure AF1. FMS image and analysis, Hole 1114A. Vertical scale = 1/200. From left: (1) depth, (2) static FMS image, (3) dynamic FMS image with a 2-m color equalization sliding window with sinusoids corresponding to the structural measurements, (4) structural interpretation tadpoles, and (5) caliper measurements. The thin vertical green line on the FMS images indicates the orientation of pad 1, which correspond to the C1 caliper reading. The tadpole position on the horizontal axis indicates the dip magnitude, and its tail points toward the dip direction. (Continued on next three pages.)

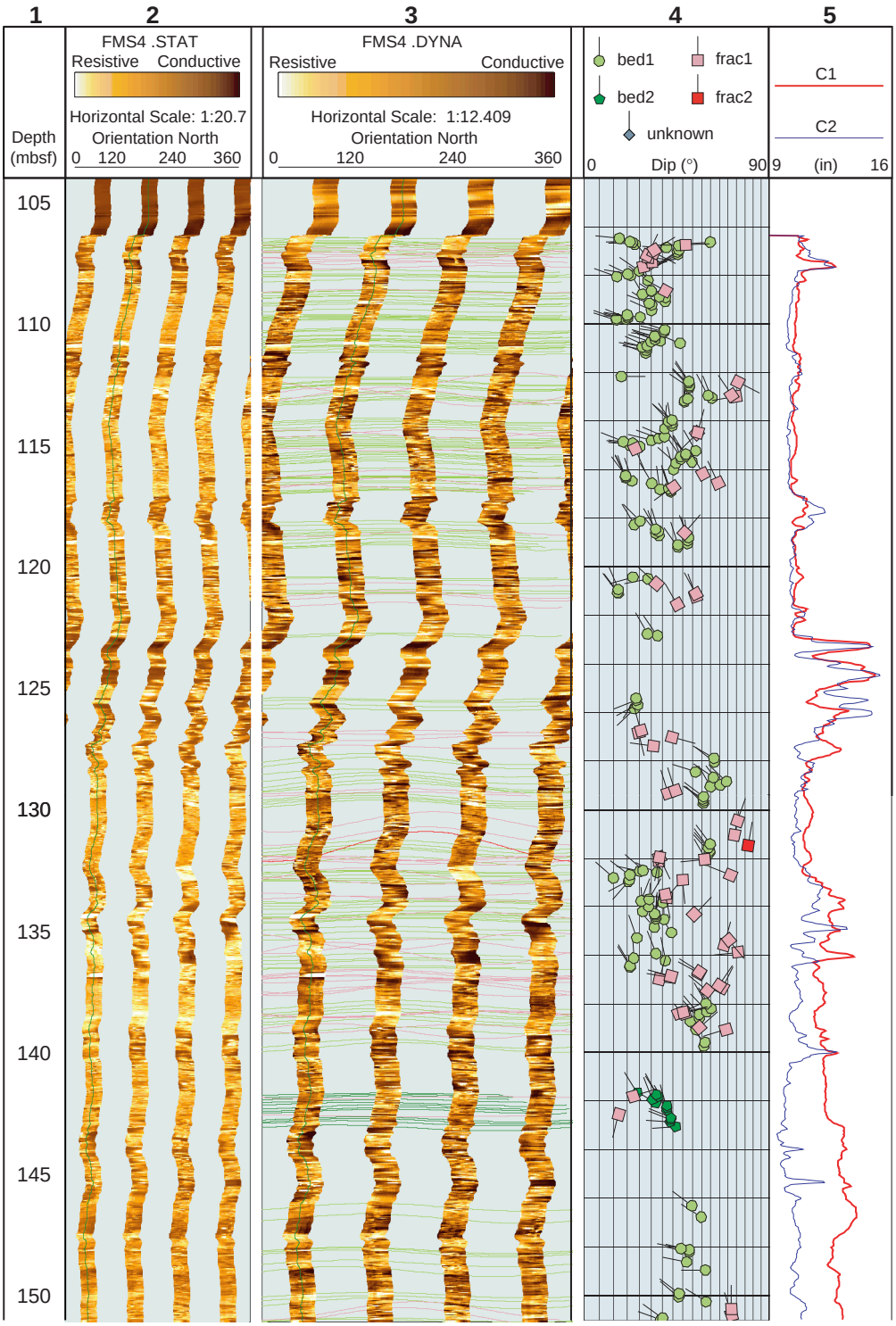

Figure AF1 (continued).

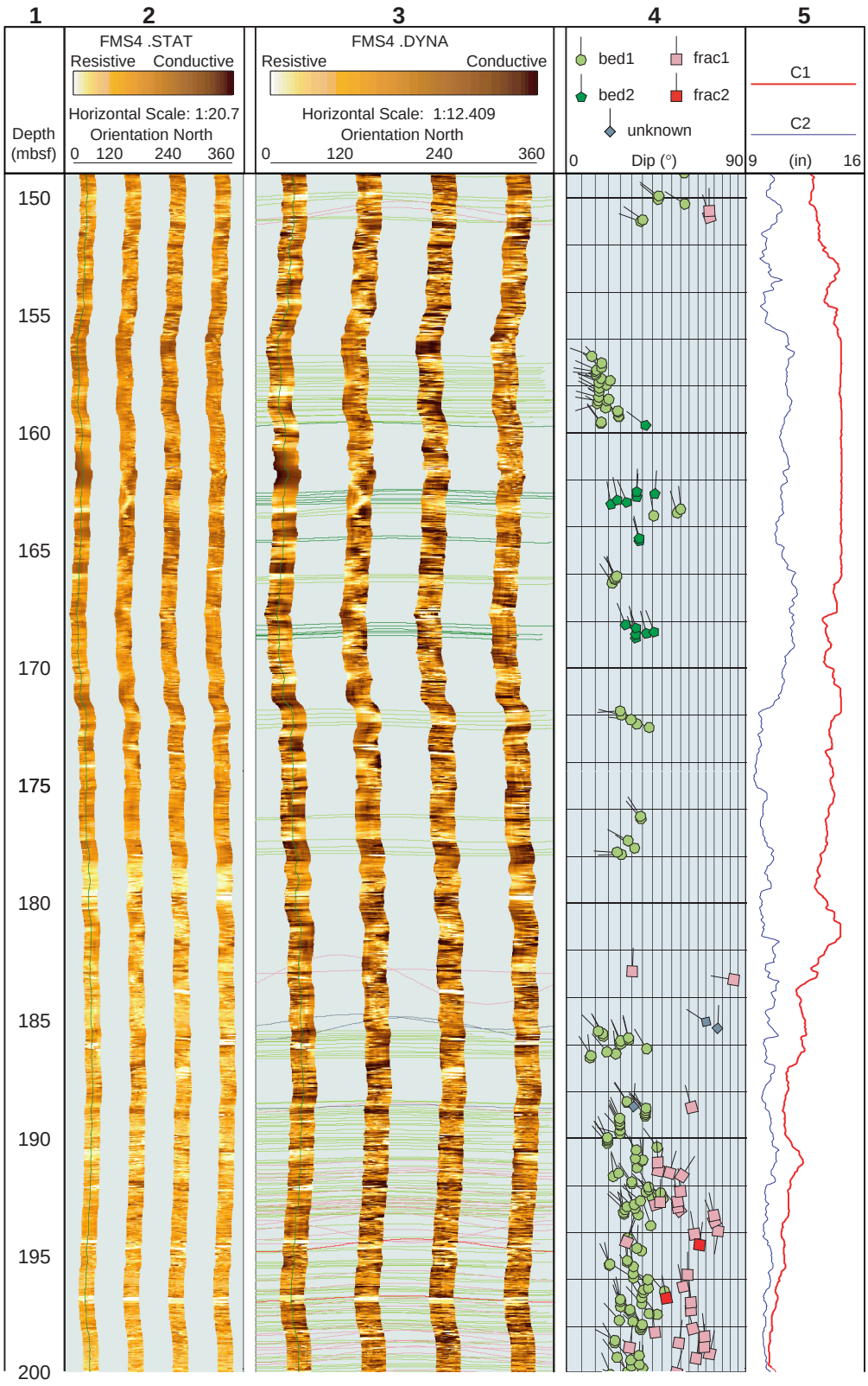

Figure AF1 (continued).

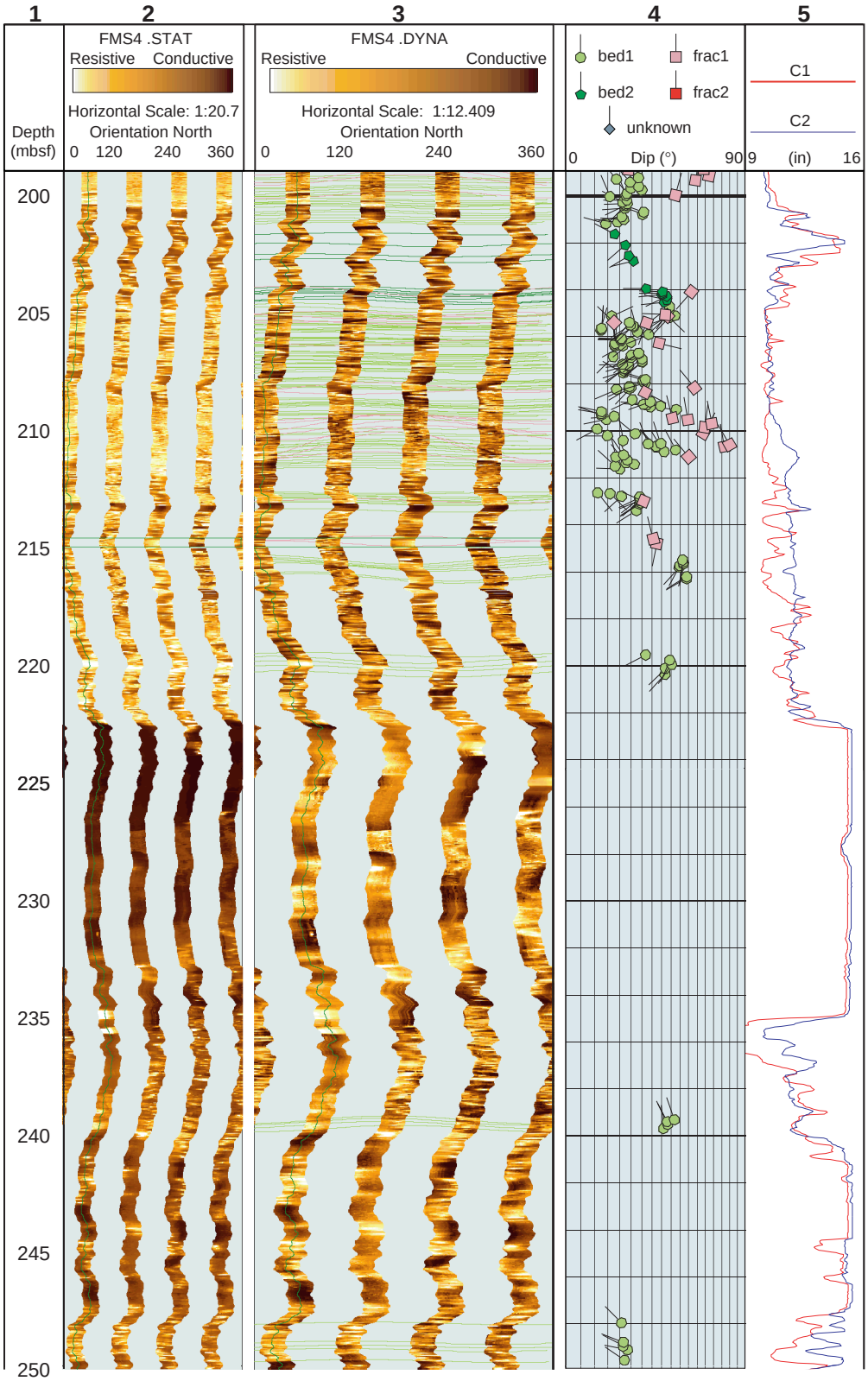

Figure AF1 (continued).